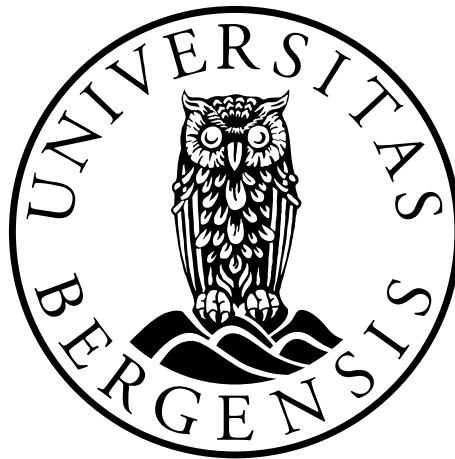


***In vitro* study of the effect of cabozantinib (XL184) on canine oral melanoma cell lines**

Caroline Sørensen Singam



This thesis is submitted in partial fulfilment of the requirements for the degree of Master in
Medical Biology - Biomedicine

Department of Biomedicine

University of Bergen

Spring 2017

Acknowledgements

First of all, I would like to thank my supervisor professor Frits Thorsen for guidance and help through this project. Thank you for taking the time to correct this thesis, giving feedbacks, and answering all my questions along the way. I have enjoyed being a member of your research group. I would also like to thank all the employees on the 6th floor at the BBB for helping me with practical questions.

I am especially grateful to Synnøve Nymark Aasen, Kislay Roy, Anna Marie Moe and Halala Sdik Saed for practical guidance on experiments in the laboratory. I am grateful for all the time you have spent teaching me new techniques and machines.

Thanks to Hege Avsnes Dale and Endy Spriet for helping me obtaining good confocal pictures. I would also like to thank Brith Bergum for good guidance with the flow cytometer instruments.

I would also like to thank Dr. Lars Prestegarden and Senior Bioengineer Anne Fossas for helping me in finding information regarding treatment procedures used against oral melanoma in the Norwegian hospitals. Thanks to Dr. Thor Christian Aase Johannessen for guidance when I struggled with my western blots.

I would also like to thank Runar Hårklau for great cooperation during our master projects, and for helping me and encouraging me in times where the lab work did not work out as planned.

Finally, I would like to thank my family for all support. Especially my mother-in-law Anne Fossas who took great interest in my project. I would also like to thank Kristian for all his support and encouragement throughout this project.

Caroline, May 2017.

Table of contents

1.	INTRODUCTION	12
1.1	MALIGNANT OM: INCIDENCE FOR HUMANS AND CANINES	12
1.2	CANINE OM CELL LINES AS A MODEL FOR HUMAN OM	13
1.3	OM: GENETIC ALTERATIONS.....	15
1.4	DIAGNOSTIC AND THERAPEUTIC PROCEDURES FOR OM IN NORWAY.....	17
1.5	CABOZANTINIB.....	19
1.6	EXPERIMENTAL METHODS.....	25
2.	AIMS	30
3.	MATERIALS AND METHODES	31
3.1	CELL LINES USED IN THIS THESIS	31
3.2	GENERAL CELL CULTURE WORK.....	33
3.3	EXPERIMENTAL PREPARATION.....	34
3.4	CELL VIABILITY ASSAYS	35
3.4.1	<i>Resazurin viability assay</i>	35
3.4.2	<i>Viability pictures</i>	37
3.5	APOPTOSIS ANNEXIN V ASSAY	37
3.6	CELL CYCLE ARREST ASSAY	38
3.7	CLONOGENIC ASSAY.....	39
3.8	SPHEROID EXPERIMENTS	40
3.8.1	<i>Tumour spheroid growth</i>	40

3.8.2	<i>Migration assay</i>	42
3.9	WESTERN BLOTTING.....	42
4.	RESULTS	47
4.1	CELL VIABILITY ASSAYS	47
4.2	APOPTOSIS ANNEXIN V ASSAY	51
4.3	CELL CYCLE ANALYSIS	53
4.4	CLONOGENIC ASSAY	54
4.5	SPHEROID EXPERIMENTS	56
4.6	WESTERN BLOTS	64
5.	DISCUSSION	66
5.1	CELL VIABILITY ASSAYS	66
5.2	APOPTOSIS ASSAY.....	67
5.3	CELL CYCLE ASSAY	69
5.4	CLONOGENIC ASSAY	70
5.5	SPHEROID EXPERIMENTS	71
5.6	WESTERN BLOTS	73
5.7	CONCLUDING REMARKS.....	75
5.8	FUTURE ASPECTS.....	76
	REFERENCES	78

List of figures

Figure 1.1- Prevalence of human and canine OM

Figure 1.2- Signal pathways involved in OM

Figure 1.3- Structure of cabozantinib

Figure 1.4- Mechanism of action of cabozantinib

Figure 1.5- Reduction of resazurin

Figure 1.6- Basic principle of flow cytometry

Figure 1.7- Basic steps in western blotting

Figure 3.1- Viability assay layout

Figure 3.2- Analysis of cell cycle using FlowJo software

Figure 4.1- Resazurin viability graphs

Figure 4.2- Cell viability pictures

Figure 4.3- Cell viability pictures

Figure 4.4- Cell viability pictures

Figure 4.5- Cell viability pictures

Figure 4.6- Cell viability pictures

Figure 4.7- Annexin V apoptosis graph

Figure 4.8- Cell phase distribution

Figure 4.9- Clonogenic pictures

Figure 4.10- Quantification of clonogenic ability after treatment

Figure 4.11- M1 spheroid growth during 21 days

Figure 4.12- M2 spheroid growth during 21 days

Figure 4.13- M3 spheroid growth during 21 days

Figure 4.14- M4 spheroid growth during 21 days

Figure 4.15- M5 spheroid growth during 21 days

Figure 4.16-migration of M2

Figure 4.17-migration of M2

Figure 4.18-migration of M2

Figure 4.19-migration of M2

Figure 4.20- live/ dead staining of spheroids

Figure 4.21- Western blots

Abbreviations

Abbreviations	Full name
AJCC	American Joint Committee of Cancer
AKT	Protein kinase B
ANG1	Angiopoietin- 1
ATP	Adenosine triphosphate
BCA	Bicinchoninic acid, often used for determining the total protein concentration in a solution
BRAF	B-Raf proto-oncogene
BSA	Bovine serum albumin
CSPG-4	Chondroitin sulphate proteoglycan
DMEM	Dulbeccos modifies eagle medium
DMSO	Dimethyl sulfoxide
ECL	Chemiluminescence
EthD-1	Ethidium homodimer-1, red fluorescent viability indicator
EtOH	Ethanol
FBS	Fetal bovine serum
FCS	Fetal calf serum
FDA	Food and Drug Administration
FITC	Fluorescein isothiocyanate, a fluorochrome often applied in flowcytometry
FLT3	Receptor-type tyrosine-protein kinase FLT3
G0/G1	Rest phase/ first phase of the cell cycle

G2/M	second subphase of interphase in the cell cycle/ mitosis
HGF	Hepatocyte growth factor
HIF	Hypoxia inducible factor
IC₂₅, IC₅₀, IC₉₀	The effluent concentration that shows a 25%, 50%, 90% reduction in toxicity
IFN-α	Interferon type 1- alfa
IκBa-NF-kb pathway	Nuclear factor kappa-light-chain-enhancer of activated B cells
JAK	Janus kinase
KIT	Mast/stem cell growth factor receptor, also known as proto-oncogene c-Kit or tyrosine-protein kinase Kit or CD117, a receptor tyrosine kinase
MAPK	Mitogen activated protein kinase pathway
MART-1	Melanoma antigen recognized by T-cells 1
MER	Proto-oncogene tyrosine-protein kinase MER, a receptor tyrosine kinase
MET	Tyrosine-protein kinase Met or hepatocyte growth factor receptor, a receptor tyrosine kinase
MilliQ	Autoclaved water
MST	Median survival time
NRASQ61	A mutation resulting in an amino acid substitution from a glutamine to a lysine at position 61 in NRAS
OM	Oral melanoma, malignant melanoma of mucosal origin in the oral cavity
P1GF	Placental growth factor

PBS	Phosphate-buffered saline
PD-1	Programmed cell death protein 1
PEN-STREP	Penicillin/streptomycin
PFA	Paraformaldehyde
PI3K	Phosphoinositide-3-kinase pathway
PI	Phosphoriodide, a viability dye staining DNA
PS	Phosphatidylserine, a component of the cell membrane
PTB	Phosphotyrosine binding domain
PTEN	Phosphatase and tensin homolog
RAS	Family of retrovirus-associated DNA sequences, part of the MAPK pathway
Resazurin	7-Hydroxy-3 <i>H</i> -phenoxazin-3-one 10-oxide
RET	Rearranged during transfection, a receptor tyrosine kinase
RIPA buffer	Radioimmunoprecipitation assay buffer, a lysis buffer used to lyse cells and tissue
RNase	Ribonuclease
ROS1	Proto-oncogene tyrosine-protein kinase ROS, a receptor tyrosine kinase
RTK	Receptor tyrosine kinase
SD	Standard deviation
SDS	Sodium dodecyl sulphate
SCF	Stem cell factor
SF	Scatter factor
SH2	Src homology region

SOX2	SRY (sex determining region Y)-box 2, a transcription factor that is essential for maintaining self-renewal of undifferentiated embryonic stem cells
S-phase	Synthesis phase of the cell cycle
STAT	Signal transducer and activator of transcription
TBS	Tris-buffered saline
TBST	Tris-buffered saline with 0.1 % tween
TIE-2	Tunica interna endothelial cell kinase, a receptor tyrosine kinase
TNM	TNM, Classification of Malignant Tumours staging system
TrkB	Tropomyosin receptor kinase B, also known as tyrosine receptor kinase B
TYRO3	Tyrosine-protein kinase receptor
VEGF	Vascular endothelial growth factor
WESTOP	Western Society of Teachers of Oral Pathology Banff Workshop classification
WHO	World Health Organization

Summary

Cabozantinib is a RTK inhibitor with main purpose to inhibit the VEGFR, KIT and MET receptors. The FDA has recently approved cabozantinib in the treatment of advanced renal cell carcinoma and metastatic medullary thyroid cancer. Oral melanoma (OM) tends to generate metastases early in disease development, but patients rarely experience early symptoms. This in turn results in a poor prognosis. Biological behaviour and treatment response is often similar in both humans and dogs, in addition dogs develop OM more frequently than humans, which makes canine an excellent animal model to study disease development and treatments. The goal of this study was to investigate the anti-cancer efficacy of cabozantinib on canine OM cell lines.

In vitro experiments were done by studying cell viability, apoptosis, cell cycle, spheroid growth, cell outgrowth from spheroids, clonogenic potential, and signaling pathways of selected RTKs in canine melanoma cells after cabozantinib treatment. For this purpose, general subculture techniques, flow cytometry, light- and confocal microscopy as well as western blots were used.

The results showed that cabozantinib reduced cell viability with IC₅₀ doses in the low μ M range. Cabozantinib treatment induced apoptosis, and decreased spheroid outgrowth and metastasis. Colony formation and cell cycle distribution was not affected by low doses of cabozantinib. When spheroid growth was observed for 21 days, low doses of cabozantinib reduced growth for all cell lines. Western blots revealed that the p-MET level was not influenced by cabozantinib treatment, however p-KIT levels were decreased for all cell lines.

In conclusion, we found that cabozantinib exhibited antitumour effects on our canine OM cell lines *in vitro*. These results indicate that cabozantinib may also be applied in a *in vivo* setting for humans and animals. Because this study only explored the effect of cabozantinib on the KIT and MET pathways, data do not exclude the possibility that cabozantinib block other pathways, resulting in the favorable effect seen on tumour behavior.

1. Introduction

1.1 Malignant OM: Incidence for humans and canines

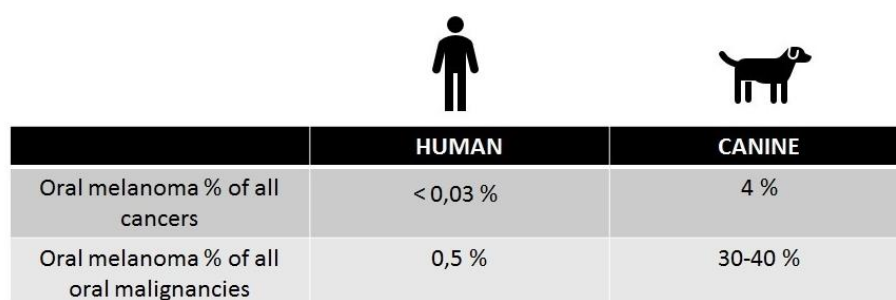
Malignant melanoma of mucosal origin in the oral cavity is a rare and aggressive neoplasm arising from melanocytes. Melanocytes can be found in the basal layer of the epithelium, where they produce the pigment melanin in specialized organelles called melanosomes. During embryogenesis melanocytes migrate to the skin, hair follicles, retina and to various mucosal membranes. In skin, melanocytes play a protective role against the harmful effects of ultra violet (UV) radiation from sun exposure, but in mucosa their function is still unclear. Mucosal melanoma is a rare form of melanoma, and accounts for approximately 1 % of all melanoma cases [1, 2]. Normally mucosal melanoma arise in the head and neck region (55 %), but it can also arise in the anal/rectal region (24 %), female genital tract (18 %) and in the urinary tract (3 %) [1]. Roughly 2 % of all head and neck mucosal melanomas are expected to be found in the oral cavity [3]. Oral melanoma (OM) makes up 0.5 % of all oral malignancies (figure 1.1) [4].

OM affects the upper aerodigestive tract, and the tumours are frequently found in sites of the hard palate or the maxillary gingiva in humans [5]. The clinical presentation of OM ranges from macular, nodular to ulcerated, where ulcers are associated with an advanced stage of the disease with development of metastasis [6]. The neoplasm is irregularly shaped with variable colour shades, depending on the pigmentation distribution. Lesions are usually black in colour with shades of dark blue, grey or brown, but non-pigmented lesions also exist called amelanotic melanoma [2, 7].

The aetiology of OM is still unknown, but factors including tobacco use, chronic irritation and environmental carcinogens are possible risk factors mentioned in the literature, but not confirmed [4]. The average age of affected patients is 55 years, ranging between 22-88 years old. Patients typically lack symptoms and with a neoplasm arising in the oral cavity, the disease is often discovered and diagnosed at an advanced stage [8]. In general, mucosal melanomas behave more aggressively than cutaneous melanoma. Due to early and aggressive

vertical growth, metastasis rates are high with frequent relocation to lymph nodes (10-25 %) and distant sites (5-10 %) like liver, lung, bone, and brain [9, 10]. This gives patients a poor prognosis with an overall five-year survival rate at approximately 15 %, with median survival time (MST) approximately two years from the time of diagnosis [1, 4].

OM is more common in canines than in humans, and is the most common oral malignancy in dogs, accounting for 30-40 % of all oral malignancies and 4 % of all canine tumours (figure 1.1) [11]. This type of cancer is commonly seen in Scottish terriers, golden retrievers, poodles, chow-chows and dachshunds [12]. Like in humans, mucosal melanoma differs in pathobiology from cutaneous melanoma, often behaving more aggressively. Untreated dogs live only for 65 days, and metastases can be seen in 70-95 % of all cases. Lymph nodes are frequently the main site of metastasis (74 %), but development of pulmonary metastases is also common [11, 13].





	 HUMAN	 CANINE
Oral melanoma % of all cancers	< 0,03 %	4 %
Oral melanoma % of all oral malignancies	0,5 %	30-40 %

Figure 1.1- Prevalence of human and canine OM: Comparison of oral melanoma in human and canine based on percent of all cancers, and percent of all oral malignancies worldwide. The figure is made with data from [4, 12, 14, 15].

1.2 Canine OM cell lines as a model for human OM

Dogs may be regarded as appropriate and valuable models to study spontaneous tumours in humans. Thus, the dog as a model system provides an opportunity to obtain increased knowledge about cancer biology and therapeutic response. Almost half of the Norwegian

population owns a pet, and 14 % owns a dog [16]. In general, malignancies in dogs develop in the same organs as in humans, and is the main cause of death in dogs. The progression of cancer is considerably faster than in humans, and therefore results on responses to new therapeutic intervention may be obtained faster [17]. Dogs live in the same environment and are exposed to the same environmental carcinogens as humans, making such a model relevant when studying carcinogens as a possible causative factor in cancer development [18].

Dogs represent a natural outbred population with spontaneously occurring tumours, compared to inbred laboratory animals where tumours either are induced either through carcinogenic exposure or transplantation. To make laboratory animals responsive to the induced cancer, they are often immunocompromised, whereas companion animals normally have a healthy immune system. Companion animals usually get good care and have loving caregivers, who make sure their animals are in good shape with good mental health. In the United States 70 % of pet owners utilize veterinary services, and most caregivers demand the highest quality of care [17].

There is a lack of established “standard of care” for many tumours, which makes it easier and morally acceptable to attempt new forms of therapy on animals. Well-designed clinical trials involving companion animals are often more acceptable to the public, compared to laboratory animal trials and human trials. Compared to human clinical trials, animal trials are less expensive, and it is easier to expand study subjects without the concern about where to accommodate the animals. As dogs develop OM more frequently than humans, it may be possible to obtain a large study group more easily, thus providing statistically more reliable treatment results. Biological behaviour and treatment response is often similar in both humans and dogs, which makes canine an excellent animal model to study disease development and treatments [17, 19]. Studies have confirmed a significant clinical and histopathological overlap between canine and human mucosal melanomas, likely making results from canine cell lines also applicable to the human setting [20].

1.3 OM: genetic alterations

The mutations and genetic alterations leading to OM are not fully understood, and published studies lack confidence in their results due to inclusion of few patients. Because of the rarity of this disease, data on tumour behaviour and mutation status are only accessible through case reports, as large clinical series are lacking [21]. However, some mutations are associated with OM, and those will be discussed in the following.

KIT mutations are common with appearances in 39-89 % of oral mucosal melanomas [22, 23]. The KIT receptor is a tyrosine kinase receptor, which plays a vital role in proliferation, migration, and survival of cells. When mutated, the receptor can be independent of its ligand, be amplified, constantly activated, or not present. Activated KIT phosphorylates various downstream signalling pathways, such as the mitogen-activated protein kinase pathway (MAPK) and the phosphoinositide-3-kinase pathway (PI3K). Both MAPK and PI3K pathways play a pivotal role in cell proliferation and survival, and may lead to cancer if not controlled (Figure 1.2) [23].

The MAPK pathway is implicated in the progression of melanoma, and activates downstream proteins like RAS. Overexpression of RAS in 89 % of OM was reported by Rivera and colleagues, whereas no expression was detected in normal melanocytes from the oral cavity. The RAS protein was found both *in situ* and in invasive phases of OM, which could be a result of a KIT mutation, possibly activating the MAPK and PI3K pathways (Figure 1.2) [24]. In another study by Rivera and co-workers, the KIT mutation was detected in abnormal melanocytes as well as in advanced stages of OM [23]. This may indicate that the KIT mutation can be important during early development of OM, and perhaps necessary for disease development. Together, these results suggest that RAS activated by a KIT mutation may have a pertinent role in OM disease development [23, 24]. Tacastacas and colleagues compared published studies where treatment with KIT inhibitors had been used on mucosal melanoma patients with different KIT mutations. Pooled result of the study showed an overall response of 51 %, providing evidence that KIT inhibitors may be effective in this selected OM population. Still the outcome for patients remained poor, proving the

need of a more efficient therapeutic approach and effective treatment options in order to increase survival rate [25].

NRAS and BRAF mutations are relatively common in cutaneous melanoma, but highly uncommon among mucosal melanomas [26, 27], suggesting a difference in origin for these melanomas [23]. Although NRAS and BRAF mutations are rare, they still need to be considered in the pathobiology of OM, as it may contribute to tumour progression and tumourigenesis by providing an alternative molecular mechanism to disease development or progression [24]. Loss of PTEN has also been observed in 4 out of 7 dogs with OM. PTEN is a tumour suppressor gene which is an important inhibitor of the AKT and mTOR pathway [28].

Overexpression of RAS, a high rate of KIT mutations combined with NRAS and BRAF mutation and loss of PTEN indicates that overlapping molecular activities may occur in OM development and progression (Figure 1.2). The variation in mutations as well as the lack of response in molecular therapies strongly supports the conception that OM may have several other oncogenic events than what is observed in skin melanomas [24, 28].

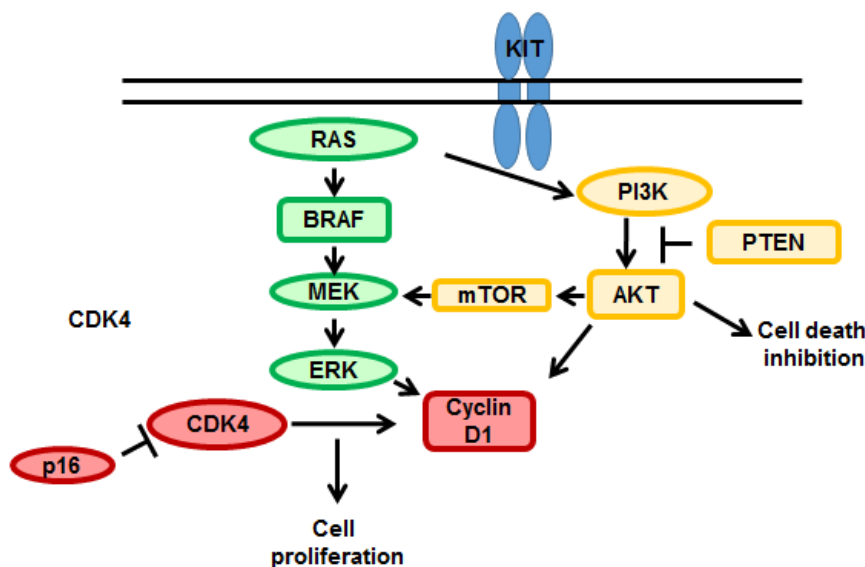


Figure 1.2- Signal pathways involved in OM: Altered KIT and overexpression of RAS leads to activation of MAPK and P13K pathways. Figure is reprinted with permission from the author Fernando Augusto and Atlas publisher [29].

1.4 Diagnostic and therapeutic procedures for OM in Norway.

OM can be difficult to diagnose, because there is a lack of standard diagnostic and therapeutic procedures as of today. There is no international established classification system, staging system or grading system for OM [1, 6]. Neither the World Health Organization (WHO) or the American Joint Committee of Cancer (AJCC) have developed systems for classifying this subtype of cancer [9]. Therefore classification, staging, and therapeutic procedures presented are based on the Norwegian national guidance procedures [30].

Classification of OM tumours

Usually the TNM Classification of Malignant Tumours (TNM) staging system of the AJCC is used to stage OM. In 2010, a new chapter of the 7th edition made by the AJCC included staging of mucosal melanoma of the head and neck, which is included in the diagnostic process of OM. In the AJCC staging protocol, mucosal melanoma staging starts at stage III, which support the concept of the advanced disease [30, 31].

OM tumours can be graded by the WESTOP (Western Society of Teachers of Oral Pathology) Banff Workshop classification. Based on their histological pattern, they are divided into *in situ* melanoma (15 %), invasive (30 %), and combined invasive melanoma with *in situ* components (55 %) [2]. Immunohistochemistry is used to confirm final diagnosis. OM shows immunoreactivity towards s-100 protein, MART-1 and tyrosinase (T311) antigens, and these are useful diagnostic tools as melanocytic differentiation markers. In cases of amelanotic melanoma, immunohistochemistry is especially important to determine the correct diagnosis, and is also used to distinguish OM from differential diagnosis, such as smoking- associated melanosis, Addison's disease, Peutz- Jeghers syndrome, amalgam tattoos and racial pigmentation [30, 32].

Treatment strategies against OM

Due to its rareness, there are no randomised clinical studies to provide any evidence-based treatment. Even though it is uncertain if surgery is the most effective treatment, extensive surgery with wide margins is the preferred treatment. Patients get further treatment with immunotherapy, based on the genetic profile of the tumours. Mucosal melanoma usually respond poorly to radiotherapy, although some authors have reported prolonged survival and local tumour control [33]. Radiotherapy is considered in advanced cases with distant metastasis, where surgery is too comprehensive [30]. Even after treatment, 20 % of the patients suffers from local recurrences, and in 45 % of the cases local recurrence with distant failure is seen [10].

Previous clinical trials have used interferon- α (IFN- α) [34], *Corynebacterium Parvum* [35], and cytotoxic treatment with dacarbazine [36], without increasing the lifespan of patients considerably.

Surgery and/or radiation therapy is also the preferred choice of treatment for canines. After surgery, the MST often correlates with the stage and the size of the tumour, which is reported to be 17–18 months for tumours of < 2 cm in diameter, 5–6 months for tumours between 2-4 cm in diameter, and 3 months for tumours > 4 cm in diameter [13, 37]. The low MST is likely due to local recurrence (42-70 %) and distant metastases (79 %) seen in dogs after surgery [38]. Treatment with radiotherapy alone or combined with chemotherapy resulted in a lower local recurrence rate (12-32 %) in the dogs, but a high rate of metastasis (around 50 %) decreased the lifetime of the affected dogs [39, 40]. Several studies on dogs have investigated different primary and adjuvant treatments, but no clinical advantage was seen in the dogs due to high occurrence of metastasis and local recurrence [11, 40-43].

Immunotherapy and cancer vaccination has been evaluated in the treatment of canine OM. Chondroitin sulphate proteoglycan-4 (CSPG-4) and programmed cell death protein 1 (PD-1) are highly expressed in canine OM, and have been evaluated for their value as immunotherapeutic targets. CSPG-4 is an important tumour antigen in human melanoma,

and can be detected in around 57 % of canine OM [44]. Vaccination with CSPG-4 antigen in resected II/III-staged CSPG4-positive dogs with OM, showed longer disease free interval with a MST of 468 days, compared to 200 days for unvaccinated CSPG-4 positive dogs. Local recurrence and metastasis rates were also decreased compared to non-vaccinated dogs, with 34,8 % vs 42 % and 39 % vs 79 % respectively [37]. PD-1 are immune checkpoint receptors that binds to its ligands on T-cells, playing a key role in suppressing the immune system and thereby enabling the tumour to evade the immune system. The receptors are activated in 90-100 % of canine OM, therefore PD-1 inhibitors may be promising as a therapeutic agent against these tumours [45]. Another strategy explored is the use of xenogeneic vaccination encoding human tyrosinase (Onecept™, Merial®, Duluth, GA, U.S.A). Two independent studies have shown induced antitumour responses in canine OM [46, 47], but a third study reported that the Onecept vaccine had no effect [48], leaving the treatment strategy disputable.

Although there are several studies investing different treatment strategies against human and canine melanomas, there is to the best of my knowledge still not a treatment able to cure OM in canines or humans. Therefore, there is still a need for developing new and improved treatment strategies.

1.5 Cabozantinib

Cabozantinib is a small-molecule tyrosine kinase inhibitor, identified as XL184 (Exelixis, South San Francisco, CA). It is chemically developed with the potential to inhibit the receptor tyrosine kinases (RTKs) KIT, MET and VEGFR, as well as several other RTKs associated with tumour pathology, including RET, ROS1, TYRO3, MER, TRKB, FLT-3 and TIE-2 receptors [49]. The structural formula of cabozantinib is shown in figure 1.3. When a malate group is added to the drug, it is orally bioavailable [50].

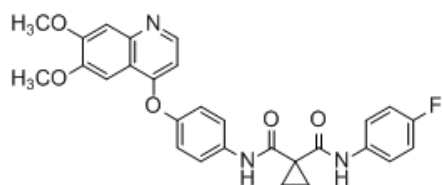


Figure 1.3- Structure of Cabozantinib: The figure illustrates the chemical structure of cabozantinib (XL182). The figure is adapted from [51].

Cabozantinib was approved by the Food and Drug Administration (FDA) in 2012 as treatment for metastatic medullary thyroid cancer and in 2016 for patients with advanced renal cell carcinoma. It is marketed as Cometriq for metastatic medullary thyroid cancer and as Cabometyx for patients with advanced renal cell carcinoma. Both medicaments are associated with severe side-effects like serious gastrointestinal fistulas and perforations, and potentially fatal gastrointestinal hemorrhage. Diarrhea and hypertension is also a common side-effect of cabozantinib consumption [52].

Cabozantinib is as of today in several trials for different malignancies, like neurofibromatosis (phase 2), castrate resistant prostate cancer (phase 2), KRAS wild-type metastatic colorectal cancer (phase 1), non-small cell lung cancer (phase 1) and triple-negative breast cancer (phase 2), among others [53, 54].

Cabozantinib is specifically designed to target RTKs. There are approximately 60 different RTKs identified in mammals, which main function is to regulate signal processes related to development, cell function and tissue homeostasis. They all share some basic structural features, and all are transmembrane glycoproteins. Their location makes them able to be activated by their cognate ligands-growth factors from outside the cell and start a signalling cascade inside the cell [55]. Ligand binding induces dimerization of the receptors, resulting in trans autophosphorylation of each other's tyrosine side chains within the cytosolic side. Autophosphorylation means the transfer of the γ -phosphate of ATP to the hydroxyl group on tyrosine. This will cause a conformational change on the tyrosine side chain, resulting in generation of binding sites for adaptor proteins bearing a Src homology region (SH2) or a

phosphotyrosine binding domain (PTB domain). When adaptor proteins are bound and activated, they continue downstream signalling in one or several cascades ending in the nucleus with altered gene expression [56]. Strict regulation of RTK activity is essential to prevent unwanted signalling. Mutations, gene rearrangement or gene amplification of both receptor and ligand can cause dysregulation of RTKs, and have been implicated as causative factors in development and progression of numerous cancers [57]. As mentioned, cabozantinib target the RTKs; MET, VEGF and KIT receptors, among others. Their function in cancer and therapeutics will be discussed further below.

MET

The ligand of MET is the hepatocyte growth factor/scatter factor (HGF/SF), and is essential for normal embryonic development, as well as epithelial to mesenchymal transition, cell migration and invasion, cell proliferation and survival, angiogenesis and morphogenic events, both in embryonic and adult life. The signalling pathways of MET can be activated when the receptor is bound to HGF/SF (Figure 1.4). All pathways stimulate growth and cell survival, and make MET to an oncogene. The different signaling pathways are activated depending on which adaptor proteins that are bound to the phosphorylated tyrosine kinase. The phosphorylated tyrosine side chain functions as a multidocking site for several adaptor proteins, which in turn recruit several signal transducing proteins to form a signalling complex that continue downstream signalling until reaching the nucleus [58].

MET signals through four major pathways; the MAPK pathway, PI3K pathway, Signal transducer and activator of transcription 3 (STAT3) pathway and the nuclear factor kappa-light-chain-enhancer of activated B cells (I κ Ba-NF-kb) pathway (figure 4.1). All pathways stimulate to growth, and contribute to tumour development if MET is dysregulated.

MET can become dysregulated by several mechanisms that result in cancer development. In normal cells, HGF/SF is a paracrine factor produced by mesenchymal cells. Some cancers get activated in a ligand dependent manner where cells express both HGF/SF and MET,

resulting in a constitutive activation of MET and its downstream signalling pathways. This autocrine loop promotes tumour development with an invasive behaviour, and is associated with a poor prognosis. HGF is produced and secreted as pro-HGF, and needs to be enzymatically cleaved to function as a growth factor. Proteins with such activity have been detected in some tumours, but their mechanism in tumour development remains to be established [59].

MET can also be activated by ligand-independent mechanisms. Overexpression of MET by gene amplification, enhanced transcription, or posttranscriptional mechanisms have been observed in tumours. Increased presence of MET receptors in the cell membrane increases the risk of spontaneous MET dimerization. This is generally not sufficient to trigger MET activation, but if transactivated by other membrane receptors they can be activated. Such clusters of dimerized MET get inhibited by suppressor molecules, but in tumour cells these may be inactivated, stimulating oncogenic development and progression [59].

Chromosomal rearrangement of MET is also a causal factor for tumour development. One oncogenic form of MET is the TPR-MET fusion which encodes an oncogenic hybrid protein that constantly activates MET [60]. Absence of normal negative regulators of MET can also lead to constitutive MET activation and tumourigenesis. In metastatic B16 melanoma cells, phosphatases that normally are responsible for MET dephosphorylating, internalization, and degradation of MET are downregulated, leaving MET to be constitutive activated [61].

Finally, several somatic or inherited mutations in the MET gene can lead to an oncogenic and typically ligand-independent edition of MET contributing to cancer [59].

VEGFR

It is established that angiogenesis is critical for tumour growth and invasion, and it is one of the hallmarks of cancer [62]. Vascular endothelial growth factor (VEGF) and its receptors VEGFR 1, 2, or 3 is responsible for this pathway in many cancers. Solid tumours can grow

up to the size of 1–2 mm before they start lacking oxygen and nutrients. They are dependent on angiogenesis for further growth, which is the development of new vasculature from existing blood vessels. In malignancy, VEGF is often constantly activated, either by a mutation leading to this constant activation, or by tumour driven upregulation of VEGF expression by pro angiogenesis factors, such as VEGF-A, placental growth factor (PlGF) and angiopoietin-1 (ANG1) [63]. Tumour cells consume less oxygen than normal cells, and normally they rely on a higher glycolysis to maintain ATP level. Nevertheless they need adequate levels of oxygen, if not the cells will get into a hypoxic state activating hypoxia-inducible transcription factors (HIFs) through the HIF pathway that stimulates angiogenesis [64]. In one way or another, tumour cells overcome hypoxic conditions by maintaining adequate oxygen levels. The formation of vasculature from existing blood vessels are often referred to as the angiogenetic switch and will continue as long as the tumour grows. The newly formed vessels will grow towards the tumour and infiltrate it. Newly formed vasculature are often leaky, making it easier for cancer cells to invade and migrate through the blood circulation [65].

Due to the importance of angiogenesis in cancer, different angiogenic inhibitors have been developed. VEGFR was an attractive target which was thought to have effect on the metastatic potential of cancer cells, as well as decreasing the tumour size. However, evidence suggest that VEGFR therapy alone fails to induce tumour remission, and the result is often the opposite of what should be expected. After treatment with VEGFR inhibitors in mice with pancreatic carcinoma local invasiveness and metastases were developed [66]. Recent evidence also suggests that tumours can become resistant to antiangiogenic drugs, possibly through alternative pathways such as MET, but also due to genetic mutations and instabilities associated with tumour cells [67]. In contrast, dual inhibition of VEGFR and MET with cabozantinib has been successful in reducing tumour size and invasiveness, and has inhibited the development of metastases [68, 69].

KIT

KIT is the receptor of the stem cell factor (SCF) and plays a significant role in regulating red blood cell production, lymphocyte proliferation, mast cell development and function, melanin formation, and gamete formation. The receptor is expressed in hematopoietic progenitor cells, mast cells, germ cells, interstitial cells of Cajal, melanocytes, and in some human tumours [70]. SCF has been proven to activate the MAPK pathway, the PI3K pathway, the JAK/STAT pathway, and the Src signaling pathway (Figure 1.4) [71, 72]. These pathways are important in cell migration and proliferation, angiogenesis and cell invasion, as well as apoptosis and cell survival.

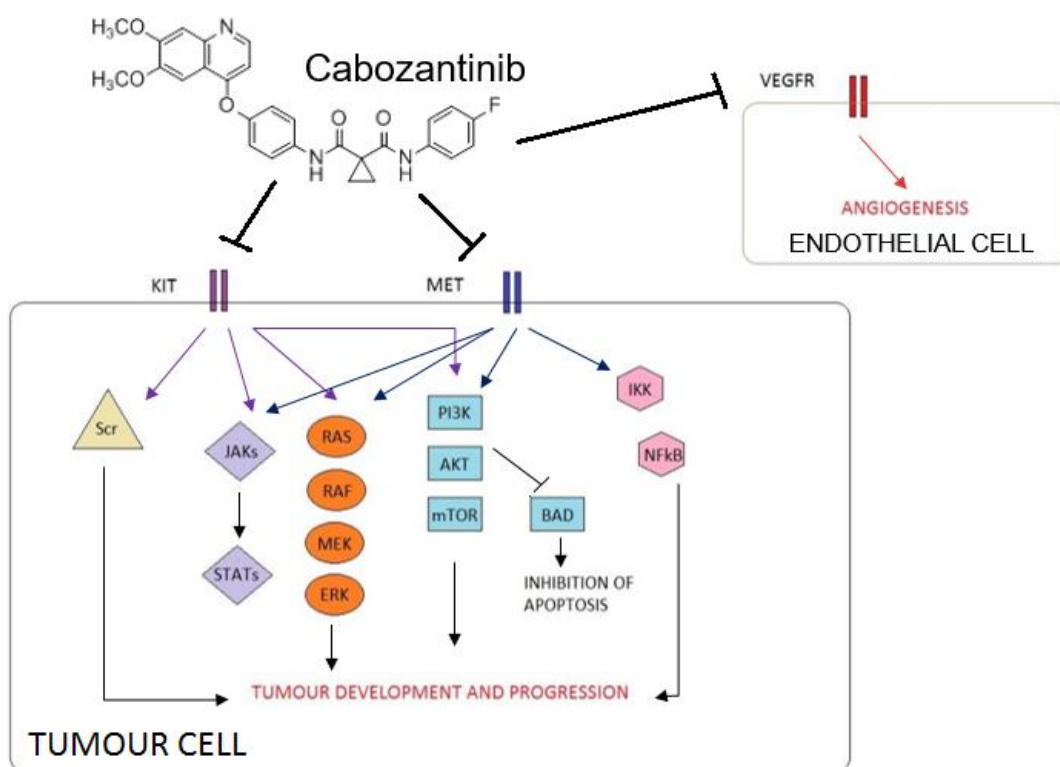


Figure 1.4- Mechanism of action of Cabozantinib: Simplified overview of pathways inhibited by cabozantinib. VEGFR is important for angiogenesis. KIT and MET can activate the MAPK pathway (orange), the PI3K pathway (blue) and the JAK/STAT pathway (purple). KIT can also activate Src signaling (yellow), while MET can activate the NFkB pathway (pink). The figure is made with data from [51, 55, 58, 64, 71, 72].

Abnormal KIT expression or function has been reported in several human diseases. Autocrine loops where the tumour produces both the KIT receptor and SCF, have been seen in some tumours. Interestingly, both gain- and loss of function mutations have been seen in tumours, including melanoma [22, 73]. KIT was originally considered to be a tumour suppressor gene, based on the decreasing protein level observed in *in situ* components compared to invasive components. However, increased KIT or SCF expression clearly have an oncogenic role in some melanomas, including OM [74].

Studies show that targeting only VEGFR or only KIT can result in MET activation [67, 75]. As KIT is known to be implicated in OM, and VEGFR is important for angiogenesis, cabozantinib serves as a strategical drug. By targeting all three receptors, the risk of inducing resistance may be decreased.

1.6 Experimental methods

A variety of methods to assess viability of cultured cells and cytotoxicity of anticancer drugs exist. The assays and methods used in research should be reliable, sensitive, reproducible and inexpensive to perform [76]. Basic principles of some *in vitro* assays and methods used in this paper are discussed in the following chapters.

Viability assay

A viability assay is a fast and reliable method to study drug efficiency on cancer cells. Several classical assays exist for measuring cell survival and proliferation, but resazurin is perhaps the most convenient one. The resazurin dye provides a simple, reliable, and rapid method to measure cell viability with low costs and high reproducibility. Resazurin can be reduced into resorufin, a pink fluorescent dye which can be measured using a microplate

reader (Figure 1.6). This reduction of resazurin in growth media is in direct correlation with the quantity of living organisms present. It is likely the oxygen consumption from metabolizing cells that causes the reduction of resazurin, although it has been suggested that mitochondrial enzymes can be responsible for the reduction [77]. It is not known whether the chemical reaction takes place inside the cell or in the medium. Regardless of the mechanism of action, the assay is reliable and proven to be a useful tool to measure cell viability [78].

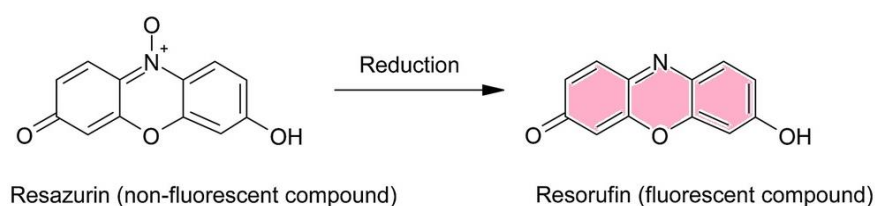


Figure 1.5- Reduction of resazurin: Non-fluorescent resazurin is reduced into fluorescent resorufin in direct correlation with the quantity of living organisms present. The figure is modified and used with permission from [79].

Basic principles of flow cytometry

Flow cytometry is a method to analyse single cells in a suspension. A light beam is focused in the observation region. Forward and side scattered light will be deflected from the cells, and fluorescence of different wavelengths can be recorded in addition (Figure 1.7).

Typically, one to six or more fluorescence colours can be measured through different filters (FL1 to FL6). Forward scatter gives information about the cell size, while side scattered light reflects granularity of the cells. Samples can be stained with fluorescent chemicals or antibodies to label components of the cell. Data are processed to give information about the different populations within a sample [80].

Flow Cytometry

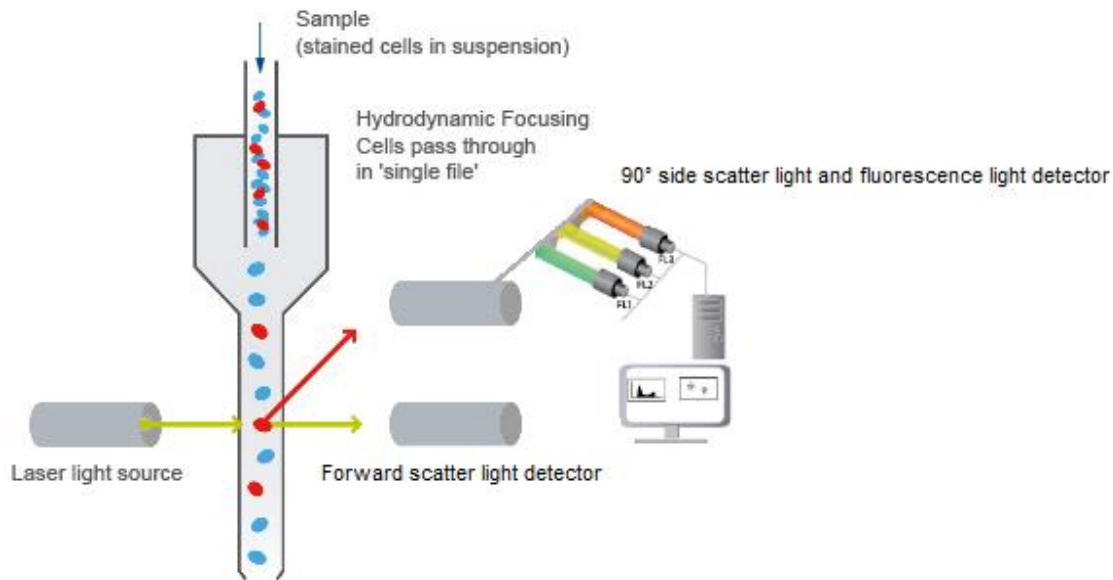


Figure 1.6- Basic principle of flow cytometry: Cells in fluid pass through the light of a laser which illuminates the cells. Forward and 90° side scattered light as well as fluorescence is detected and analysed by a computer. The illustration is created with figures from [81, 82] and with permission from © Abcam plc.

DNA analysis is one of the most important applications of flow cytometry. Cells are fixed and stained before measurement of DNA content to give information about the cell cycle distribution. Cells are typically stained with propidium iodide (PI), which targets the DNA [83].

Flow cytometry is frequently combined with annexin V staining to measure apoptotic cells. Phosphatidylserine (PS) is a phospholipid and a component of cell membranes. In healthy cells PS is facing the cytosolic side, but during apoptosis these PS get “flipped” to facing the outside of the cell membrane. Annexin V is a calcium dependent phospholipid-binding protein with high affinity towards PS, and can therefore be used as a probe to detect apoptosis. In necrosis PS will also be “flipped”, but the cell membrane will not be intact as during apoptosis. Annexin V is normally fluorescence isothiocyanate (FITC)-labelled (green

fluorescence) and used in combination with a vital dye such as PI to distinguish apoptotic and necrotic cells. Living cells with intact membranes exclude PI, whereas the membranes of dead and damaged cells are permeable to PI. Based on this information, living cells are both annexin V and PI negative, while cells that are in early apoptosis are annexin V positive and PI negative, and late apoptotic or dead/ necrotic cells are positive for both annexin V and PI [84, 85].

Western blotting

Western blotting is a powerful tool to immunodetect proteins after electrophoresis. Using a sodium dodecyl sulphate (SDS) polyacrylamide gel, proteins can be separated based on molecular weight. Once separated, proteins can be transferred to an absorbent membrane, forming an exact replica of the gel. Antibody probes targeting the membrane bound proteins can be added for the immunodetecting of the proteins of interest. A secondary antibody with fluorescence or with conjugated enzyme activity/ enzyme substrate is added, making it able to visualize the band of the protein of interest (Figure 1.8). Intensity of the visualized band is in correlation with the amount of the protein [86, 87].

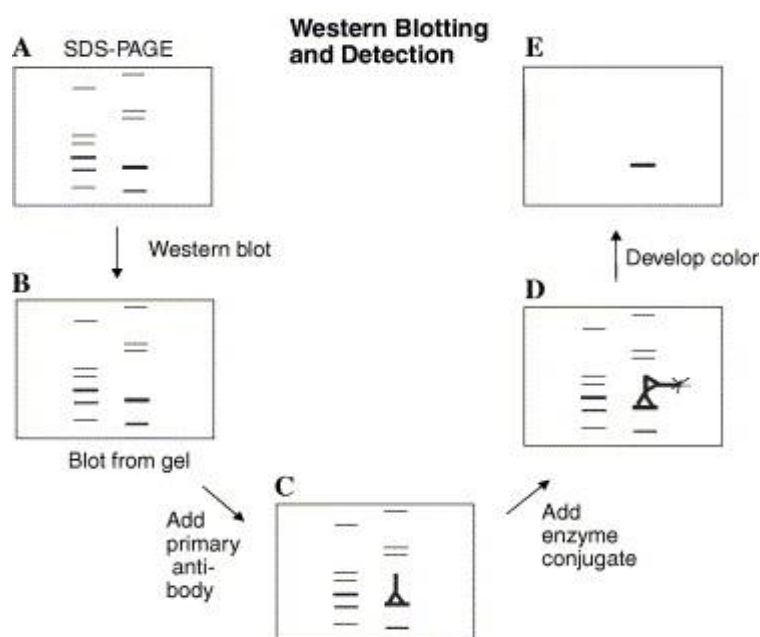


Figure 1.7- Basic steps in western blotting: (A) Proteins are separated using SDS–PAGE gel prior to Western blot. (B) Proteins are transferred to an absorbent membrane. (C) Primary antibody binding to a specific band on the blot. (D) Secondary antibody conjugated to an enzyme of fluorescence binds to primary antibody. (E) Visualization of specific band showing the protein of interest. The figure is reprinted with permission from [87].

2. Aims

OM is a rare, but highly mortal disease which affects both humans and companion animals. Standard care of patients is lacking, and no effective treatment is developed to cure the disease. For this purpose, the University of California at Davis have harvested cells from canines with OM, which are used in this project. This project is part of a larger program at the Kristian Gerhard Jebsen Brain Tumour Centre at the Department of Biomedicine, University of Bergen, where one of the main research fields is brain metastasis.

The main aim of this master thesis is for the first time to study the effects of cabozantinib in the treatment of canine OM. If successful, this drug can be one step closer to offer an efficient treatment for OM in dogs, as well as in humans.

Two sub-aims have been defined for this thesis:

1. Evaluate the anti-cancer efficacy of cabozantinib as a potential therapeutic agent against canine OM cell lines based on ability to:
 - a. reduce cell survival and inhibit cell proliferation
 - b. reduce tumour spheroid size and migration
 - c. induce apoptosis and cell cycle arrest in canine OM cells
2. Evaluate if cabozantinib effectively inhibits VEGFR, MET and KIT receptors, by studying the effect on the phosphorylated form of these receptors.

3. Materials and Methodes

3.1 Cell lines used in this thesis

Five different cell lines; UCDK9M1, UCDK9M2, UCDK9M3, UCDK9M4 and UCDK9M5 from canine OM were used in this thesis, all provided by Dr. M. Kent from the University of California at Davis. For simplicity, the cell lines will be referred by their two last characters (M1-M5) in the following. The M3 cell line is a pulmonary metastasis, and the M4 cell line is generated from a skin regrowth of OM. The remaining three cell lines are metastases from lymph nodes (M2, M5) and (M1) from a skin lesion. Information about the different cell lines are described in table 3.1. Gender, age and breed for each cell line is listed, as well as information about the tumour origin.

Table 3.1- Canine cell lines: Information concerning gender, age, breed, and tumour origin from dogs used in this paper.

Cell line	Gender	Age	Dog breed	Biopsied from	Biopsy date	Growth rate
M1	Male	17	Mini poodle	Skin metastasis from OM	9/13/2000	Rapid
M2	Male	11	Irish terrier	Lymph node metastasis from OM	10/6/2000	Slow
M3	Female	15	Springer spaniel/Chow chow cross	Pulmonary metastasis from OM	10/10/2000	Medium
M4	Male	8	German short haired pointer	Biopsy from regrowth of OM from 9 months earlier	N/A	Medium
M5	N/A	N/A	N/A	Lymph node metastasis from OM	1/30/2000	Medium

Status on some mutations and proteins belonging to M1-M5 cell lines has been published previously. Chon and colleagues concluded that the canonical Wnt/ β catenin pathway is not activated in these cell lines, suggesting that targeting β -catenin has poor therapeutic potential [88]. Wei and co-workers tested the cell lines for BRAF and NRAS hot spot mutations. The M5 cell line tested positive for the NRAS Q61 mutation, whereas the other cell lines did not bear any of these mutations [89]. Information about expressed proteins found in all of the cell lines M1-M5 are presented in table 3.2.

Table 3.2: List of proteins expressed in all cell lines M1-M5 from published articles.

Proteins expressed	Reference
p-ERK1/2	[88, 89]
p-AKT	[88]
Bim	[88]
p-Bad	[88]
Bcl-x	[88]
Mcl-1	[88]
Cyclin E	[88]
Cyclin D1	[88]
p-Rd	[88]
mTOR	[88]
p-86	[88]
p-4E-BP1	[88]
eIF4e	[88]

3.2 General cell culture work

All cell lines were cultured with ALT DMEM growth medium (see table 3.3) in culture flasks with filtered caps (25, 75 or 175 cm², Thermo Scientific, Nunc, Roskilde, Denmark). Flasks were stored in an incubator at 37 °C with 5 % CO₂ and 100 % humidity. All work involving cells was performed in a sterile environment inside a laminar flow cabinet bench, prewashed with 70 % ethanol. Solutions frequently used for cell culture are listed in table 3.3.

Table 3.3: Solutions frequently used for cell culture.

NAME	SUPPLIER
ALT DMEM:	
- 450 mL Dulbeccos modified eagle's medium	Sigma-Aldrich Inc., St. Louis, MO, USA
- 50 mL Heat inactivated fetal calf serum (FCS)	Fischer Scientific, MA, USA
- 10 mL L-Glutamine, 200 nM	BioWhittaker, Verviers, Belgium
- 10 mL Penicillin/Streptomycin (PEN-STREP), 100 µL/mL	BioWhittaker, Verviers, Belgium
- 16 mL Non-essential amino acids 100X	BioWhittaker, Verviers, Belgium
- 0,1 mL Plasmocin 25 mg/mL	Invitrogen, CS, USA
Dulbeccos phosphate- buffered saline (PBS) 10 X *	Sigma-Aldrich Inc., St. Louis, MO, USA
Trypsin EDTA, 0.25%	BioWhittaker, Lonza, Verviers, Belgium
Dimethyl sulfoxide (DMSO), >99 %	Sigma-Aldrich Inc., St. Louis, MO, USA
Cabozantinib XL 184 (>99% chemical purity)	ChemieTek, Indianapolis, USA
Blue filter cap sterile flasks: 25 cm ² , 75 cm ² and 175 cm ²	Thermo Scientific, Nunc, Roskilde, Denmark

*1X PBS used in this thesis is made from 10X PBS diluted in autoclaved milliQ water.

During the experiments flasks were regularly trypsinated and sub-cultured when almost confluent. This was done by removing old growth medium, then cells were washed twice with 0.04 mL/cm² 1x PBS (Sigma Aldrich Inc. St. Louis, MO, USA) before 0.017 mL/cm² trypsin were added (BioWhittaker, Lonza, Verviers, Belgium). Cells were further incubated until detached from the flask, then 0.06 mL/cm² ALT DMEM (see table 3.3) was added to inhibit the effect of trypsin. Further, 30-500 μ L of the trypsinated cells were transferred into a new flask with 0.17 mL/cm² growth medium, and placed in an incubator.

When cells were not used, they were cryopreserved and stored in liquid nitrogen at -196 °C. This was done by centrifugation of the trypsinated cells for 4 minutes at 900 rpm. The supernatant was removed, and the cell pellet was resuspended with freezing solution consisting of 10 % Fetal Bovine Serum (FBS) (Life Technologies, Gibco, South America), 10 % DMSO (Sigma Aldrich, St. Louis, MO, USA) and 80 % ALT DMEM (see table 3.3), then aliquoted into 1 mL cryotubes (Thermo Scientific Inc., MA, USA) and frozen in -80 °C for at least 24 hours before stored in liquid nitrogen. Cells from cryotubes were thawed as required. The freezing solution was then removed by centrifugation, and the cell pellet was resuspended with 5 mL ALT DMEM and transferred into 25 cm² growing flasks containing 10 mL ALT DMEM. When confluent, the cells were transferred to 75 or 175 cm² flasks.

3.3 Experimental preparation

In all experiments cells were grown in 175 cm² flasks (if not stated differently) and used for experiments when reaching 70-90 % confluency. To make a cell suspension, cells were trypsinated and then centrifuged, before the supernatant was discarded to keep the cell suspension free of trypsin. Cells were counted using 0.4 % trypan blue (Life technologies, Eugene, OR, USA) with CountessTM automated cell counter (Invitrogen, Oregon, USA) using the manufacturers protocol, described elsewhere [90].

All experiments were done in triplicates, and untreated control cells (negative control) were always used. Pure (99 %) cabozantinib (ChemieTek, Indianapolis, USA) was dissolved in 99 % DMSO (Sigma Aldrich) to make a 200 mM stock solution. ALT DMEM (table 3.3) was used to dilute cabozantinib concentrations further. The highest concentration of DMSO in cabozantinib treatments was 0.05 % DMSO. Therefore 0.05 % DMSO controls were also used in some experiments to ensure that this did not affect tumour cells. Dissolved cabozantinib stock (200mM) was stored in -20 °C for maximum 4 months, and diluted concentrations of cabozantinib with ALT DMEM were stored in -20°C for maximum 3 weeks.

3.4 Cell viability assays

3.4.1 Resazurin viability assay

To test cell survival after treatment with cabozantinib, a resazurin viability assay was performed on all cell lines. Cells in monolayer were treated with different concentrations of cabozantinib, ranging from 1 pM to 100 μ M to study cell viability after 72 hours of treatment.

Cell suspensions containing 25 000 or 30 000 cells pr. mL, depending on growth rate of the cell lines, were used to fill a 96-well plate (Thermo Scientific, Nunc, Roskilde, Denmark). 100 μ L of the cell solution were added to each well, except the outer borders which were filled with 100 μ L ALT DMEM. After 24 hours of incubation, 100 μ L cabozantinib were added to the wells to give the following concentrations; 0 μ M (negative control), 1 pM, 10 pM, 100 pM, 1 nM, 10 nM, 100 nM, 1 μ M, 10 μ M and 100 μ M, see figure 3.1. The drug concentrations of cabozantinib were made using series of 1:10 dilutions with ALT DMEM, to maintain a low concentration of DMSO. Plates with drug, as well as negative controls and DMSO controls were added in six replicates and the experiment was repeated three times for each cell line (figure 3.1).

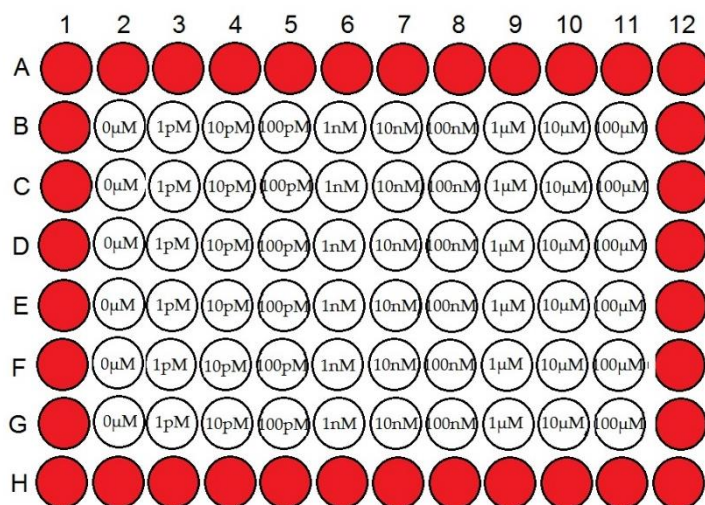


Figure 3.1- Viability assay layout: Cabozantinib concentrations ranging from 1 pM to 100 μ M were added to the cells. The outer borders were filled with ALT DMEM. Plates with DMSO controls were also made (not shown in the figure).

After adding the drug, the plates were further incubated for 72 hours, before 20 μ M of 0.1 mg/mL resazurin was added. Resazurin was made by dissolving resazurin sodium salt (Sigma-Aldrich, MO, USA) with 1X PBS (Sigma-Aldrich Inc.). The cells were incubated for 4 hours with resazurin before scanning with multiwall spectrophotometer (VictorTM 1420 multi-label counter, Perkin Elmer, Waltham, MA, USA) at excitation 560 nm/ emission 590 nm. The software WorkOut 2.0 (Dazdag Solution, Perkin Elmer, Waltham, MA, USA) was used to calculate the readout values.

The background signals from medium and resazurin were subtracted to correct the data. The viability values were converted into percent viability, where control samples were used as a reference to determine 100 % viability for each cell line. The data was further analysed using Graph Pad Prism v7 software (GraphPad software Inc., San Diego, CA, USA). X- values were transformed into their logarithmic form and Y values were normalized. The data were fitted to a normalized response – variable slope logistic nonlinear regression analysis. The data transformation demonstrated the cell viability relative to the drug concentration. Graph

pad calculator was used to calculate IC₂₅, IC₅₀ and IC₉₀ doses of cabozantinib for all cell lines.

3.4.2 Viability pictures

To confirm the findings from the resazurin viability assay, pictures were taken with and without live/dead staining (Molecular Probes, Eugene, OR, USA).

Cells were seeded in the same manner as with the resazurin viability assay (see chapter 3.4.1). After 24 hours, cells were treated with their respectable IC₂₅, IC₅₀ and IC₉₀ dosage of cabozantinib, DMSO control or negative control. After 72 hours of incubation pictures were obtained with a Nikon TE2000 light microscope (Nikon Instruments Inc., NY, USA), using the 10X objective. In addition, pictures were taken after 30 minutes of incubation with 2 μ M calcein (Molecular Probes) and 4 μ M ethidium homodimer-1 (EthD-1) (Molecular Probes) staining. These two dyes are affected by intracellular esterase activity and plasma membrane integrity respectively. The dye was added directly to wells containing cells and ALT DMEM.

3.5 Apoptosis Annexin V Assay

To evaluate if cabozantinib can induce cell death, an annexin V apoptosis assay was done and analysed with flow cytometry.

For this assay 75 000 cells were seeded into each well of a 6-well plate (Thermo Scientific, Denmark). When the plates were confluent, the growth medium was removed and the cells were treated with cabozantinib equal to their IC₂₅, IC₅₀ or IC₉₀ doses, and incubated for 72 hours. At the day of analysis, medium from each well were transferred to sterile 10 mL centrifuge tubes. 1mL of 1X PBS was used to wash the cells before they were harvested by trypsination. 1X PBS from the cell wash, as well as trypsinated cells were transferred to the

tube containing medium, and centrifuged for 5 min at 1000 rpm, ensuring collection of both floating dead cells, apoptotic cells, and living cells.

The supernatant was discarded and the cell pellet was resuspended with 50 μ L annexin binding buffer (10 mM HEPES (Sigma-Aldrich, St. Louis, MO, USA), 140 mM NaCl (Sigma-Aldrich, St. Louis, MO, USA) and 2.5 mM CaCl_2 (Merck, Darmstadt, Germany, PH = 7.4). Then 2.0 μ L Annexin V (Alexa Fluor® 488 conjugate) (Thermo Scientific, Eugene, OR, USA) and 0.5 μ L of 50 μ g/mL propidium iodide (PI) (Sigma-Aldrich, St. Louis, MO, USA) were added and samples incubated at room temperature for 30 minutes, before stored on ice. After the incubation period, 200 μ L annexin-binding buffer were added before flow cytometry was performed, using a BD LSRFortessa™ flow cytometer (Becton Dickinson Biosciences, NJ, USA).

3.6 Cell cycle arrest assay

Flow cytometry was performed to measure potential effects of cabozantinib on the cell cycle.

160 000 cells pr. well were seeded in 6-well plates (Thermo Scientific, Denmark). After 24 hours of incubation, the cells were treated with their respective IC_{25} , IC_{50} or IC_{90} doses of cabozantinib. Untreated cells were used as negative controls. The cells were treated for 72 hours before they were harvested by trypsination and centrifuged at 900 rpm for 4 minutes at 4 °C. The supernatant was discarded and the cell pellet was resuspended with 3 mL ice-cold 100 % EtOH (VWR chemicals, Rue caulot, Fontenay-sous-bois, France). EtOH was added dropwise while vortexing to avoid clumping of fixated cells. Cells in EtOH were kept in the refrigerator for minimum of 24 hours before analysis.

At the day of analysis, the cells were centrifuged at 1000 rpm for 5 minutes at 4 °C. The supernatant was discarded and the pellet was resuspended in 100 μ L 1X PBS, before centrifugation at 1000 rpm for 5 minutes at 4 °C. The supernatant was again removed, and

50µL of 1 mg/mL RNase (Ribonuclease A from bovine pancreas, Sigma-Aldrich Inc., St. Louis, MO, USA) was added. Further, 150 µL PI (Sigma-Aldrich) was added before incubation for 30 minutes in room temperature, while shaded from light.

After the incubation period, the samples were stored on ice, and analysed by an Accuri C6 flow cytometer (Becton Dickinson Biosciences, NJ, USA). Populations of cells were selected (Figure 3.2 A) and 10 000 cells within this population were analysed per sample. The analysis was performed by using FlowJo software (FlowJo, LLC, Ashland, OR, USA). Single cells were further selected (Figure 3.2 B) and presented as a histogram. FlowJo software calculated percent of G0/G1, S and G2/M phase for each sample (Figure 3.2 C).

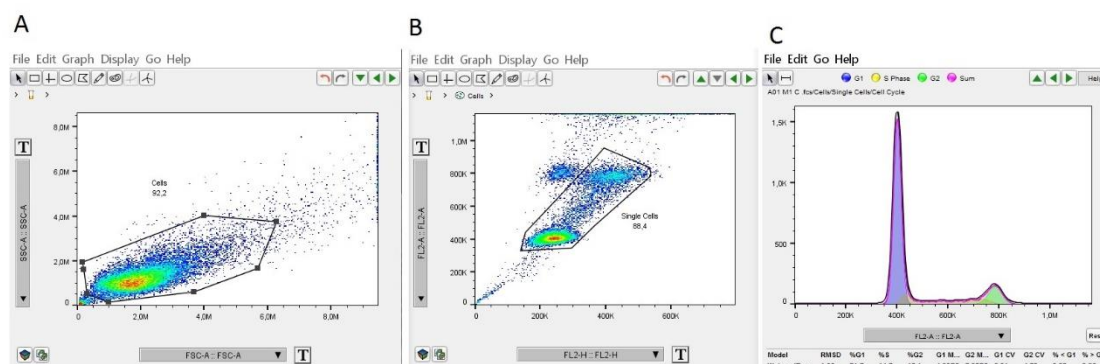


Figure 3.2- Analysis of cell cycle using FlowJo software. A) Population containing cells are selected, excluding debris and doublets. B) Population of single cells is selected. C) Data are presented in a histogram, and FlowJo calculated percent of G0/G1 (purple), S (yellow) and G2/M phase (green).

3.7 Clonogenic assay

The ability to make colonies is important in tumour progression. A clonogenic assay were done to study whether cabozantinib did inhibit colony formation of the cancer cells.

The cells were seeded in a concentration of 15 000 cells pr. well in a 12-well plate (Thermo Scientific Inc., Denmark). When the wells were confluent, the medium was removed and the cells treated with their respective IC₂₅, IC₅₀ or IC₉₀ doses of cabozantinib. Untreated cells were used as negative controls. After 72 hours of incubation, the cells were trypsinated and

counted before reseeded in a concentration at 1000 cells pr. well in a 6-well plate (Thermo Scientific, Denmark). The cells were grown for 7 days before the medium was removed and washed with 1X PBS. Thereafter, the cells were fixated with 4 % paraformaldehyde (PFA) (Thermo Scientific, Rockford, IL, USA) for 30 minutes at 37 °C. The PFA was removed before staining with 0.5 % crystal violet (Sigma-Aldrich, St. Louis, MO, USA) and 6 % glutaraldehyde (Merck Milipore, Darmstadt, Germany). The dye was removed, and cell colonies containing at least 50 cells were counted manually.

3.8 Spheroid experiments

Cell culturing in 2D monolayer vs. 3D has been compared, and there is solid evidence that 3D cultures provide a better model to study cancer which resembles tumour growth seen in patients [91-94]. Cell lines cultured in monolayer suffer several limitations. For example; 3D *in vitro* culture systems have shown to present a better model concerning drug sensitivity. 2D monolayers also lack the 3D microenvironment, cell to cell and cell to matrix interactions that are important in differentiation, proliferation, apoptosis, and gene expression. The lack of this structural architecture in 2D monolayer can be a limitation when studying signalling and protein transport procedures inside the cell. 3D models such as spheroids provides a more realistic tumour model. Taken this in account, current preclinical research heavily relies on cells cultured in monolayer as they provides an easy and convenient model and a good model to measure cell viability [93]. Therefore, both 2D and 3D models are included in this thesis.

3.8.1 Tumour spheroid growth

The spheroids were observed for 21 days after treatment with cabozantinib to study potential effects on spheroid growth after treatment.

5000 cells in 100 μ L were seeded into each well of a Corning Costar 96-well low attachment, round-bottom plate (Sigma-Aldrich, St. Louis, MO, USA), except the outer borders which were filled with ALT DMEM. The plates were centrifuged at 900 g for 15 min to form spheroids. Spheroids were grown for 6 days, before treated on the 7th day with their respective IC₂₅, IC₅₀ or IC₉₀ doses of cabozantinib, as well as a 0.05 % DMSO control and a negative control. The spheroids were observed in a microscope for 21 days, and images were taken at the day of treatment start, as well as 7, 14 and 21 days after treatment start. The pictures were taken with a Nikon TE2000 light microscope (Nikon Instruments Inc., NY, USA), using a 4X objective for the M1 and M5 cell lines, and a 10X objective for the remaining cell lines. The growth medium containing drug was changed as required during the experiment.

Live and dead staining of spheroids

4000 cells in 100 μ L were seeded into each well of a Corning Costar 96-well round bottom low attachment plate (Sigma-Aldrich). The plates were centrifuged for 15 minutes at 900 g to make spheroids. Spheroids were grown for 6 days, before treated with 100 μ L of their IC₅₀ dose. Untreated spheroids were used as negative controls. Due to time limits, this was only done for the M4 cell line. The M4 cell line was chosen because of its great ability to form spheroids.

After 72 hours of incubation, a live and dead viability/cytotoxicity kit (Molecular Probes) was used to check for cell viability. A dilution of the dye was made by adding 40 μ L of the 2 mM EthD-1 stock solution and 10 μ L of 4 mM calcein AM solution pr. 10 mL of sterile 1X PBS. 100 μ L of old growth media was removed from each well, leaving the spheroid in 100 μ L growth media. 100 μ L of diluted staining solution was added to the cells, leading to a concentration of 4 μ M calcein AM and 4 μ M ethidium homodimer-1 in each well. After incubation for minimum 60 minutes, the spheroids were transferred to chambered cover

glass system plates (Lab-Tek, Naperville, IL, USA), and pictures were taken using a Leica TCS SP8 confocal microscope (Leica Microsystems, Wetzlar, Germany).

3.8.2 Migration assay

The ability of cancer cells to migrate is important and one of the hallmarks of cancer. To test the ability to migrate after treatment with cabozantinib, a spheroid based migration assay was performed.

Spheroids containing 5000 cells were formed by centrifugation at 900 g for 15 minutes. The spheroids were grown for 7 days in Corning Costar 96-well round bottom low attachment plate (Sigma-Aldrich), before transferred to 24-well high attachment plates (Thermo Scientific Inc., Denmark) coated with collagen I (Milipore, Temecula, CA, USA) and treated with IC₂₅, IC₅₀ or IC₉₀ doses of cabozantinib, as well as negative controls (no drug). The wells were collagen I coated to improve spheroid attachment. For the coating, 204 µL collagen pr. 12,5 mL 1X PBS were used to cover all wells for minimum 30 minutes, before washing with 1X PBS twice. One spheroid was transferred to each well and two orthogonal spheroid diameters were measured on day 0, 2, 3 and 4.

3.9 Western blotting

Lysate collection

Cells cultured in 75 cm² flasks were treated when reaching 60 % confluency. IC₅₀ dose treated cells and control cells (no drug) were made for all cell lines. This was done by replacing old growth media with 10 mL of treatment solution diluted in ALT DMEM. The cells were collected 72 hours after treatment, and when cells were 80 % confluent for the control cells. The growth medium was removed and 5 mL 1X PBS were used to wash cells. 5 mL PBS was added and cells were loosened with a cell scraper (TPP Techno Plastic Products

AG, Trasadingen, Switzerland) and transferred to 10 mL centrifuge tubes. The tubes were centrifugated for 4 minutes at 900 rpm and the supernatant was removed. The pellet was resuspended with RIPA buffer (Sigma-Aldrich, St. Louis, MO, USA) together with phosphatase inhibitors (PhosSTOP EASY pack) (Roche Diagnostics, GmbH Mannheim, Germany) and protease inhibitors (cOmplete mini protease inhibitor cocktail tablets) (Roche Diagnostics, GmbH Mannheim, Germany). This was made with one tablet of phosSTOP and one tablet cOmplete mini protease inhibitor cocktail tablets pr. 10 mL RIPA buffer. This mix was made and aliquoted before stored at -20 °C, and thawed as required. 500 µL of the mix was used to resuspend the pellet, before being transferred to 1,5 mL Eppendorf tubes. The tubes were further incubated on ice for 20 minutes, and vortexed occasionally. The cells were then sonicated for 20 seconds at 30 amplitude. Further, tubes were centrifuged for 20 minutes at 4°C, before the supernatant was transferred to new Eppendorf tubes and stored in - 80 °C. The lysate was aliquoted into smaller aliquots to prevent re-defrosting.

Protein concentration measurement

For the measurement of proteins, a stock of 10 µg/µL bovine serum albumin (BSA) (Sigma-Aldrich Inc., St. Louis, MO, USA) was made to make standard series with known protein concentrations. BSA was dissolved in RIPA buffer and filtered through a sterile 0.2 µm syringe filter (Pall Corporation, Life Sciences, Ann Arbor, MI, USA). The BSA stock was diluted with RIPA buffer to make following concentrations: 0.5 - 1.0 - 2.0 - 4.0 - 5.0 µg/µL of BSA protein. PierceTM BCA protein kit (Thermo Scientific, Rockford, IL, USA) was made to make the BCA working stock, containing reagent A:B in a 50:1 ratio. 2 µL of the standard series of BSA protein concentrations, as well as samples were added to a 96-well plate (Thermo Scientific Inc., Denmark). Further, 200 µL of BCA was added to both samples and the BSA samples. The plate was then incubated for 30 minutes in the dark before analysis with a multiskanTM FC microplate photometer (Thermo Scientific Inc., MA, USA) at 562 nm. Protein concentrations were calculated based on the BSA standard curve.

Blotting

For the blotting, 25-50 µg protein from the samples were used. The amount of protein was equalized before being loaded. 5 µL of NuPAGE LDS sample buffer 4X (Novex, Carlsbad, CA, USA) and 2 µL of NuPAGE sample reducing agent 10X (Invitrogen, Carlsbad, CA, USA) was mixed with samples. The samples were then diluted with milliQ water as required, to make 20 µL. The samples were incubated on a heat block at 70 °C for 10 minutes before being loaded to a NuPAGE 4-12 % bis-tris gel, 1.5 mm, 10-well (Novex, Carlsbad, CA, USA). Fresh running buffer (50 mL NuPAGE MOPS SDS running buffer (Novex, Carlsbad, CA, USA) + 950 mL milliQ) was added to the two big chambers of the western blotting container (Novex, Carlsbad, CA, USA). The middle chamber contained 200 mL of the fresh prepared running buffer mixed with 500 µL NuPAGE ® antioxidant (methylformamide) (Invitrogen, Carlsbad, USA). The comb was removed from the cassette before 20 µL of each sample was added, as well as 10 µL of the standard SeeBlue® Plus2 prestained standard (1X) (Invitrogen, Carlsbad, USA). The outer chambers were filled with running buffer before the lid was placed on the western blotting container, and 120 V was applied for approximately 2 hours, or until standards had reached the bottom of the gel.

The cassette was opened and the gel was placed on a 0.2 µm nitrocellulose blotting membrane (GE Healthcare, Life Sciences, Germany). Two filter papers were placed on each side of the gel placed on the nitrocellulose blotting membrane. Pads, filter papers and the nitrocellulose blotting membrane was pre-soaked in transfer buffer (50 mL NuPAGE MOPS transfer buffer (20X) (Novex, Carlsbad, USA) with 850 mL milliQ water and 100 mL 100 % methanol (Honeywell, St. Louis, MO, USA). Two pads were placed in the bottom (cathode) (-) of the blotting module, before filter paper, nitrocellulose blotting membrane, gel, filter paper, and more pads were added in written order. It was important that the nitrocellulose membrane was facing towards the cathode, and the blot module was stuffed sufficiently with pads to make a resistance within the box. The anode (+) was used as a lid, and when properly assembled in the western blotting container, all chambers were filled with transfer buffer. The blotting chamber was placed in a container with ice to avoid overheating. Then 35 V was applied for 120 minutes.

After the transfer, the membrane was rinsed with ponceau solution (Sigma-Aldrich Inc., St. Louis, MO, USA) until the bands appeared. This was done to ensure that proteins had been transferred to the membrane during the transfer. The membrane was further cut into as many pieces as antibodies used on the membrane. Membrane pieces were placed in separate plastic containers, and blocked with 5 % skim milk solution (5 % Difco Skim Milk BD, Sparks, MD, USA), 95 % 1X TBST). The 1X TBST solution was made by adding 0.1 % Tween 20 (Sigma-Aldrich Inc., St. Louis, MO, USA) to 10X TBS (Sigma-Aldrich Inc., St. Louis, MO, USA), and further diluted with milliQ water. The membranes were blocked for 90 minutes on a see-saw rocker with 18-23 osc/min, before blocking solution containing primary antibodies were added. The membranes were incubated with primary antibody overnight at 4 °C in a see-saw rocker at 11 ocs/min.

The antibodies used in this thesis was p-MET antibody (Tyr1230/1234/1235) catalog nr. 07-2242 ordered from Merck Milipore, Darmstadt, Germany and p-KIT (Tyr730) polyclonal antibody catalog nr. 44-496G from Thermo Scientific Inc., MA, USA. Both primary antibodies were isolated from rabbit host.

GAPDH Antibody (0411) with catalog nr. sc-47724 from Santa Cruz Biotechnology, Dallas, Texas, USA was used as loading control. This antibody was isolated from mouse host.

All primary antibodies were diluted in 1:1000, and specified to reacted with canine cells.

After overnight incubation, the primary antibody was removed and membranes washed with 1X TBST three times for 10 minutes on a see-saw rocker at 18-23 osc/min. The secondary antibodies were further added, and the membranes were incubated for 90 minutes at 17 ocs/min in room temperature. Secondary antibodies used was anti-goat mouse (31430) and anti-goat rabbit (31462) conjugated with horse radish peroxidase, both purchased from Thermo Scientific Inc. Secondary antibodies were diluted 1:20 000 in blocking solution.

After 90 minutes, the membranes were washed with 1X TBST three times for 10 minutes, before bands were visualized with chemiluminescence (ECL) kit; West PICO or WEST FEMTO (Both from Thermo Scientific, Rockford, IL, USA) in a pre-cooled (-25 °C) darkbox

machine (Fujifilm LAS3000, Intelligent DarkBox). A 1:1 solution of ECL was added to the membranes and incubated inside the dark box for 5 minutes, before pictures was taken with 20 seconds of light exposure between pictures.

4. Results

4.1 Cell viability assays

Resazurin viability assay

A resazurin assay was done to study the effect of cabozantinib on cell viability.

Representative viability curves for the 5 cell lines are shown in figure 4.1.

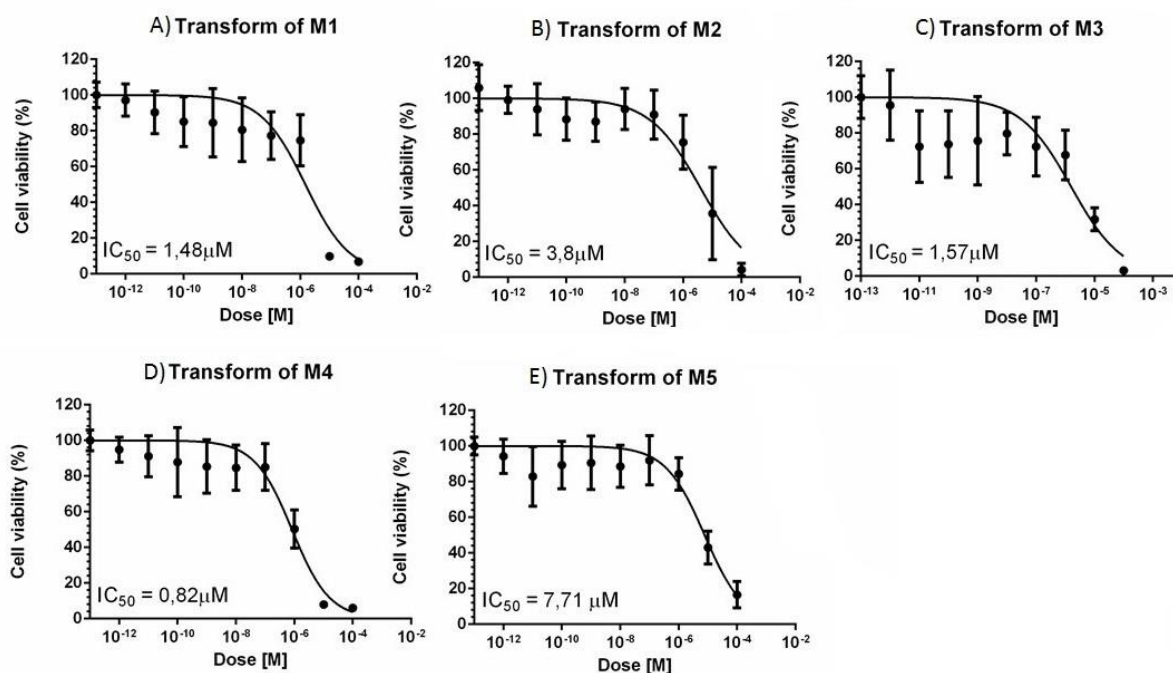


Figure 4.1- Resazurin viability graphs: Representative graphs showing cell viability after 72 hours of treatment with cabozantinib. The treatment concentrations ranged from 1 pM to 100 μM . The concentrations of cabozantinib are presented in the X-axis as log values. The IC_{50} value shown for each cell line is an average of triplicate experiments where $n=6$ (see also table 4.1). Mean \pm standard deviation (SD).

All cell lines showed increased sensitivity to cabozantinib with increasing doses. The IC_{50} values were in the low μM range for all cell lines (Table 4.1). These results indicate that

cabozantinib may have anticancer effect also on OM in an *in vivo* setting, laying the foundation for choosing treatment doses in further, preclinical experiments.

Table 4.1- IC₂₅, IC₅₀ and IC₉₀ doses of cabozantinib: Calculated IC₂₅, IC₅₀ and IC₉₀ for all 5 cell lines. Graph pad prism software was used to calculate these values.

Cell line	IC ₂₅ μ M	IC ₅₀ μ M	IC ₉₀ * μ M
M1	1,22	1,48	~100
M2	0,43	3,80	~100
M3	1,17	1,57	~100
M4	0,15	0,82	~100
M5	1,38	7,71	~100

* The highest dose of cabozantinib eradicated 80-100 % of cells, for simplicity the treatment with 100 μ M will be referred as IC₉₀ for all the cell lines in the following.

Images of viability pictures

To confirm the findings from the resazurin viability assay, brightfield pictures and fluorescence pictures of cells stained with live/dead kit (Molecular Probes) were obtained. The green-fluorescent calcein-AM indicate intracellular esterase activity in living cells and the red-fluorescent ethidium homodimer-1 indicate loss of plasma membrane integrity in dead cells. Only green fluorescence was seen in these pictures as dead cells floated freely in the growth media.

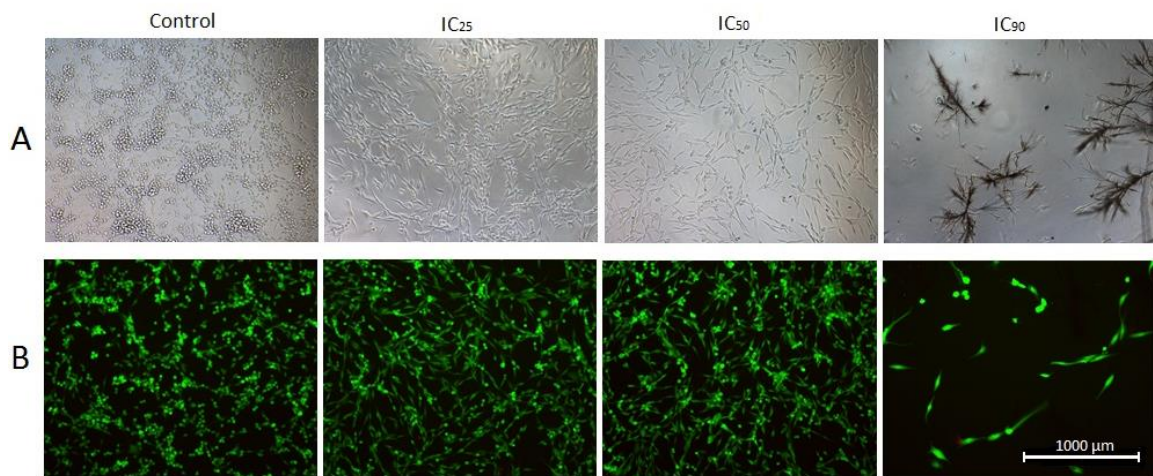


Figure 4.2- Cell viability pictures: Brightfield (A) and fluorescence (B) images of the M1 cell line treated with its IC₂₅, IC₅₀, IC₉₀ dose of cabozantinib, as well as untreated control cells.

Figure 4.2 shows that control cells of the M1 cell line grew in small clusters. Nearly 50 % of the control cells had a small and round morphology, while the remaining half were elongated. After cabozantinib treatment, the cells only showed an elongated morphology, and the cell numbers were reduced in a dose dependent manner.

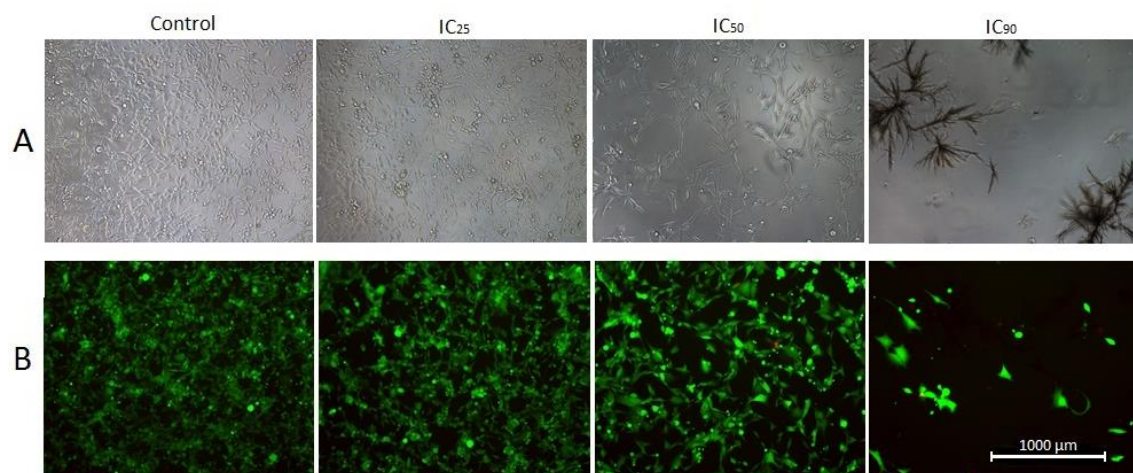


Figure 4.3- Cell viability pictures: Brightfield (A) and fluorescence (B) images of the M2 cell line treated with its IC₂₅, IC₅₀, IC₉₀ dose of cabozantinib, as well as untreated control cells.

Figure 4.3, 4.4 and 4.5 shows that the M2, M3 and M4 cell lines grows evenly distributed, with some round cells and some elongated cells. Also here, the cell numbers were decreased when treated with increasing doses of cabozantinib. Cells treated with their IC_{50} dose had more space per cell due to reduced cell numbers. This in turn gave space for enlarged growth of cells with an elongated morphology.

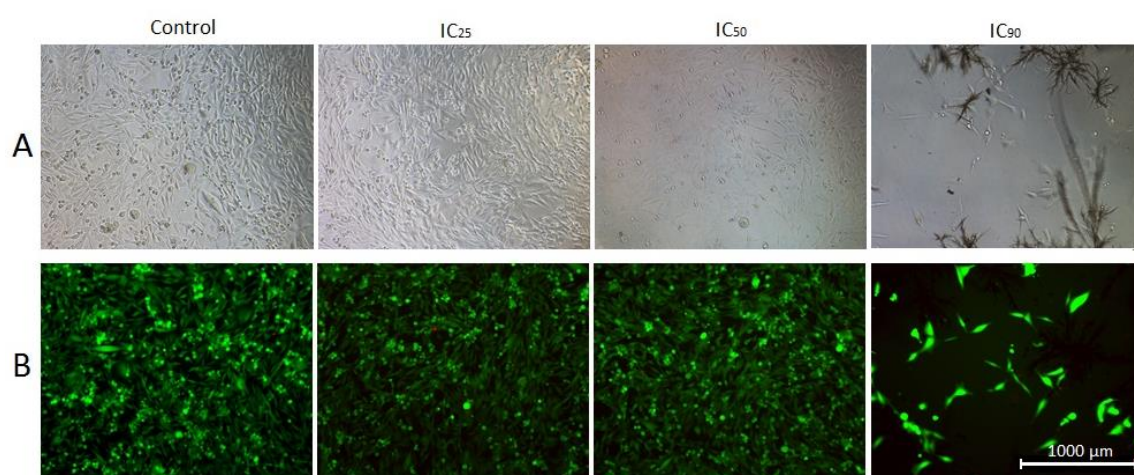


Figure 4.4- Cell viability pictures: Brightfield (A) and fluorescence (B) images of the M3 cell line treated with its IC_{25} , IC_{50} , IC_{90} dose of cabozantinib, as well as untreated control cells.

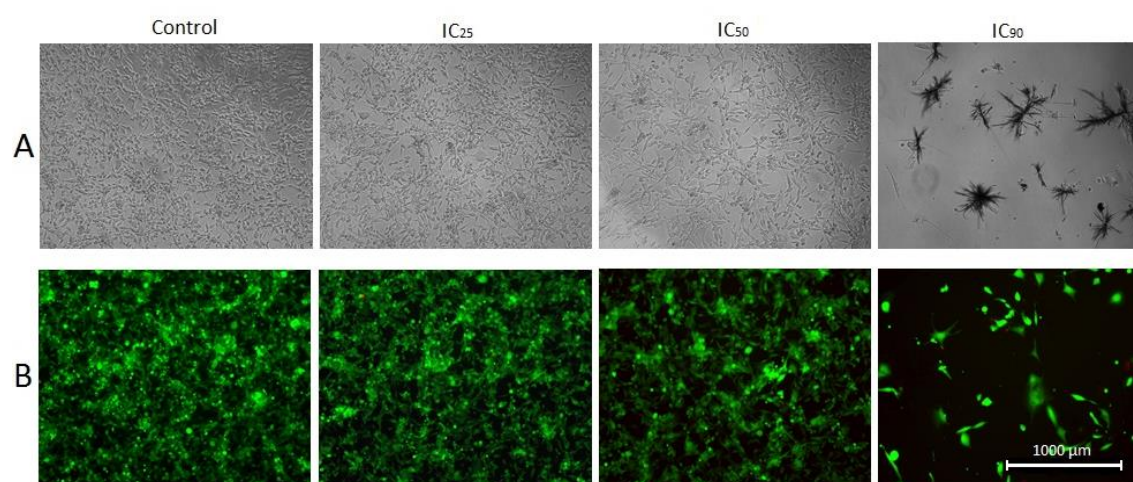


Figure 4.5- Cell viability pictures: Brightfield (A) and fluorescence (B) images of the M4 cell line treated with its IC_{25} , IC_{50} , IC_{90} dose of cabozantinib, as well as untreated control cells.

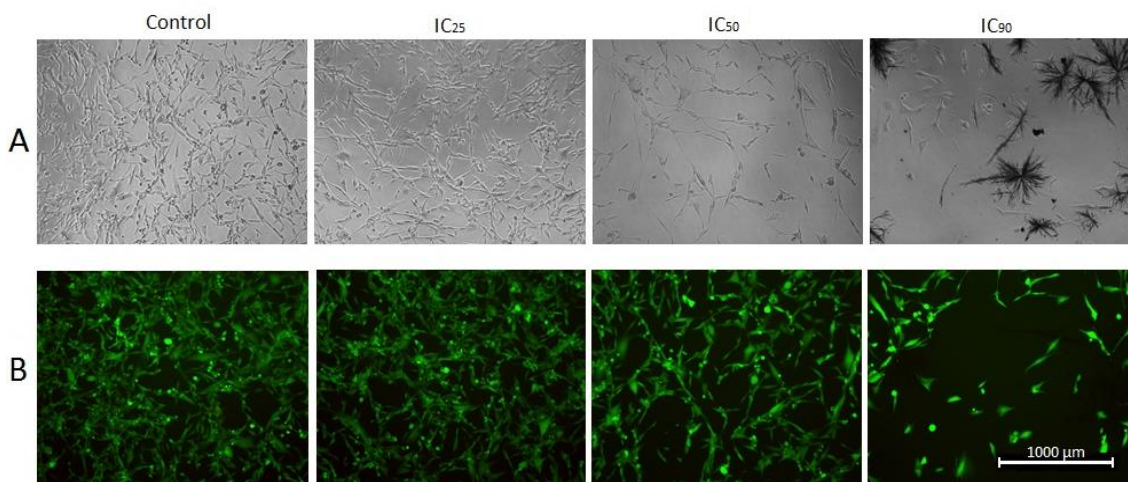


Figure 4.6- Cell viability pictures: Brightfield (A) and fluorescence (B) images of the M5 cell line treated with its IC₂₅, IC₅₀, IC₉₀ dose of cabozantinib, as well as untreated control cells.

Figure 4.6 shows that the M5 cell line grew in an elongated form. When the cell numbers were decreased, the remaining cells grew in an extensive elongated formation.

All cell lines were responding to cabozantinib in a dose dependent manner. Cabozantinib is highly lipid soluble, and thus formed crystals in the highest treatment dose (100 μ M).

Therefore, fluorescence pictures were obtained to clearly see cells treated with the IC₉₀ dose of cabozantinib. Pictures of cells treated with 0.05 % DMSO was also taken (not shown). 0.05 % DMSO did not influence the cell growth.

4.2 Apoptosis annexin V assay

The numbers of apoptotic cells after 72 hours of treatment with their IC₂₅, IC₅₀ or IC₉₀ doses of cabozantinib were analysed using flow cytometry. 10 000 cells were analysed per sample, and the percentages of live, early apoptotic, late apoptotic and dead cells for all cell lines

were determined (figure 4.7). A two-tailed students *t*-test was used to compare untreated control cells with the different cabozantinib treatments (figure 4.8).

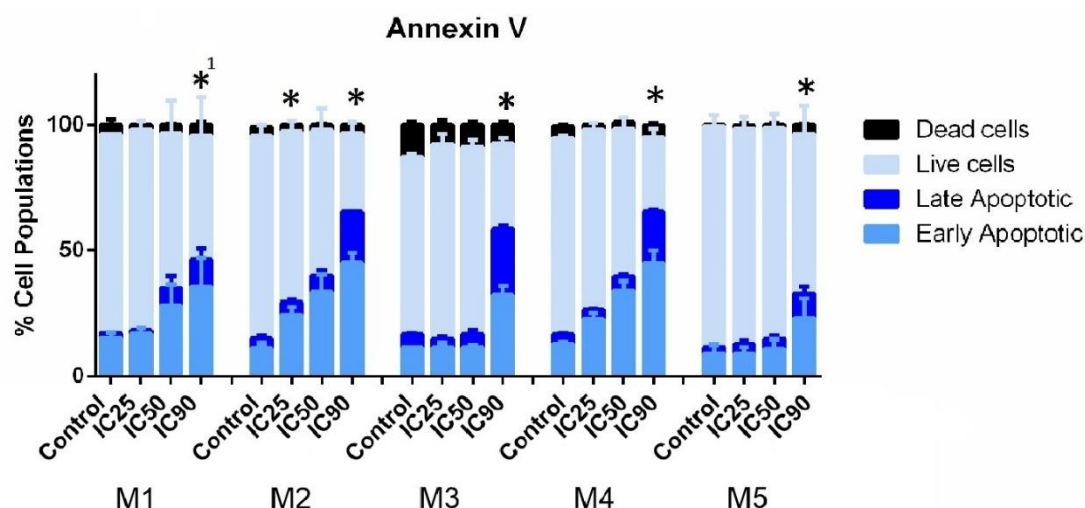


Figure 4.7- Annexin V apoptosis graphs. Percent of dead-, live-, late- and early apoptotic cells for the M1, M2, M3, M4 and M5 cell lines, after 72 hours of cabozantinib treatment. Three different treatment concentrations were used per cell line, equal to each cell lines IC₂₅, IC₅₀ or IC₉₀ dose of cabozantinib. A two tailed students *t*-test was done to evaluate statistic effects of treatments. Abbreviations: *; < 0,05, *¹; < 0,05 for all treatments was statistic significant, except the number of dead cells. Mean +/- standard deviation (SD), n=3.

In general, all cell lines exhibited a dose-dependent increase in apoptosis (figure 4.7).

Significant effects were seen in samples treated with IC₉₀, and IC₂₅ for the M2 cell line.

Although significant effect not was observed for all treatments, a clear dose dependent effect was seen for the M2 and M4 cell line. M1 cells responded to both the IC₅₀ and the IC₉₀ dose, while the M3 and M5 cells only responded to the IC₉₀ dose.

4.3 Cell cycle analysis

A cell cycle analysis was performed to see whether cabozantinib treatment resulted in changes in the cell cycle distribution. Cabozantinib treated cells were stained with PI and the DNA content was measured by flow cytometry (figure 4.8).

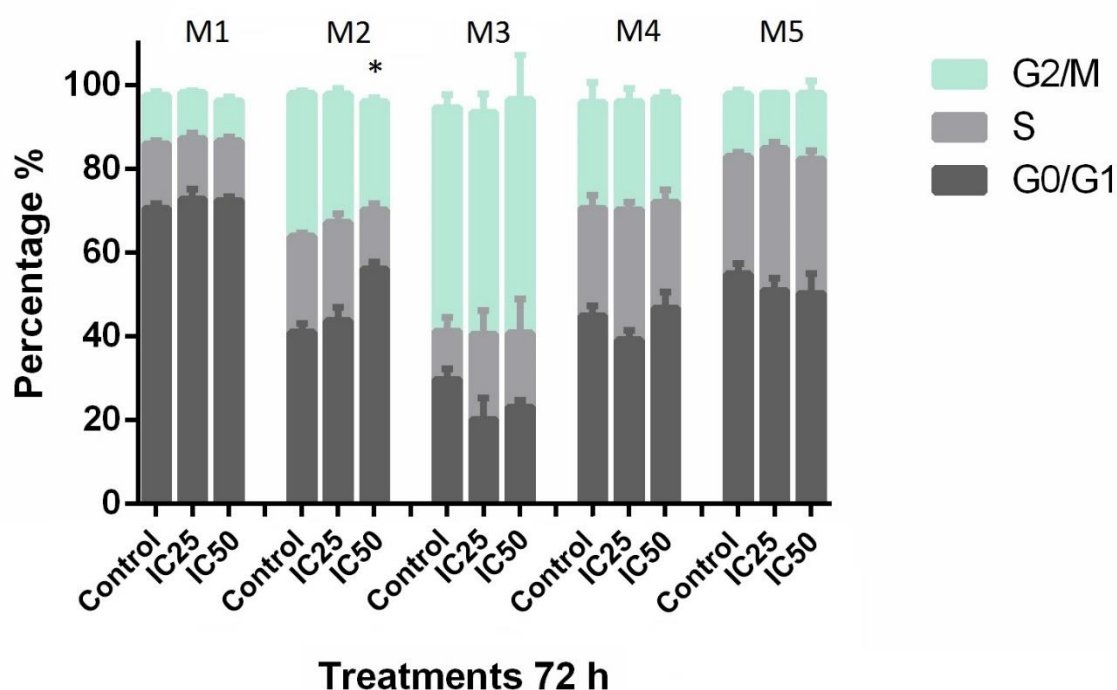


Figure 4.8- Cell cycle distribution. The amounts of G2/M, S and G0/G1 in percentages are shown for all cell lines treated with IC₂₅ dose and IC₅₀ dose of cabozantinib, as well as untreated control samples. A two tailed students *t*-test was done to evaluate statistic effects of treatments Abbreviations; * < 0,001 difference in G0/G1 phase compared to control treatment. Mean +/- standard deviation (SD), n=3.

In general, no differences in cell cycle distribution between treated and untreated cells were observed. Only the M2 cells had a significant increase with approximately 15 % more cells in G0/G1 phase after IC₅₀ treatment, compared to untreated cells. IC₉₀ was not obtained for this experiment, due to time limitations in this thesis.

4.4 Clonogenic assay

A clonogenic assay was done to study the effect of cabozantinib on the colony potential of the cells after treatment. Selected images of the most representative colonies are shown in figure 4.9, while a quantification of the number of colonies formed after treatment is shown in figure 4.10. One colony contains at least 50 cells.

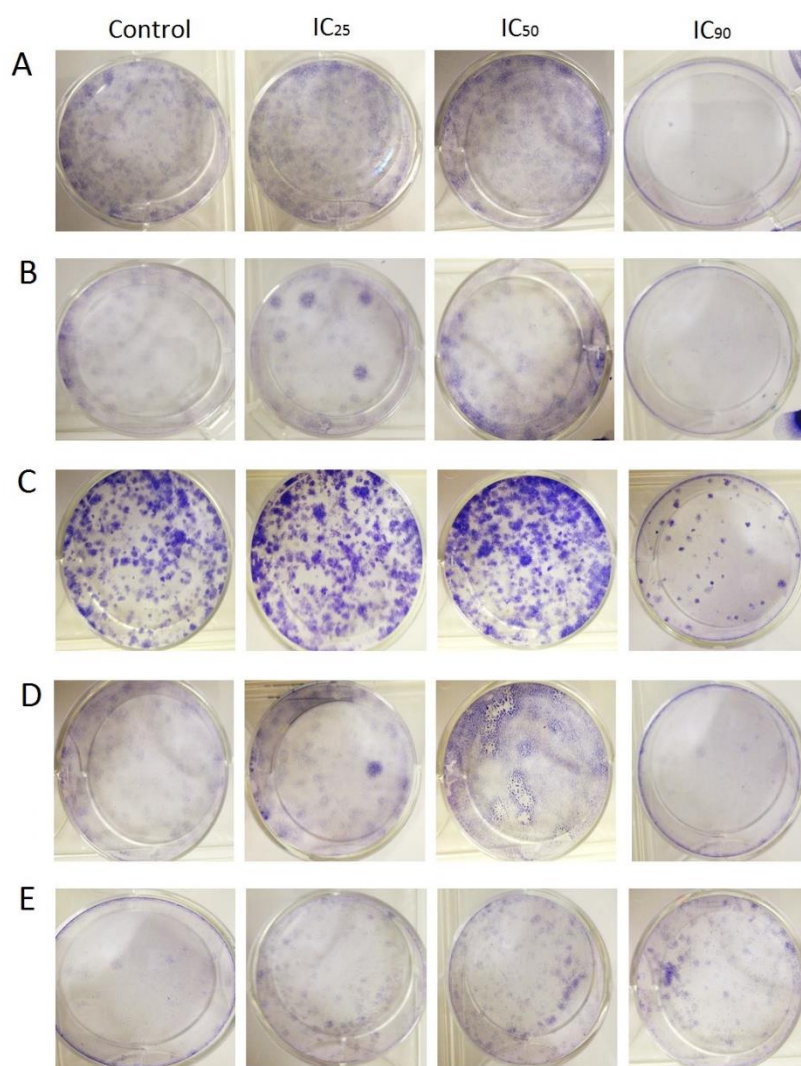


Figure 4.9- Clonogenic pictures: Formation of colonies after 72 hours of treatment with IC₂₅, IC₅₀ and IC₉₀ cabozantinib, as well as negative control wells (no treatment). Here a representative selection of images is shown for all cell lines; M1 (A), M2 (B), M3 (C), M4 (D) and M5 (E).

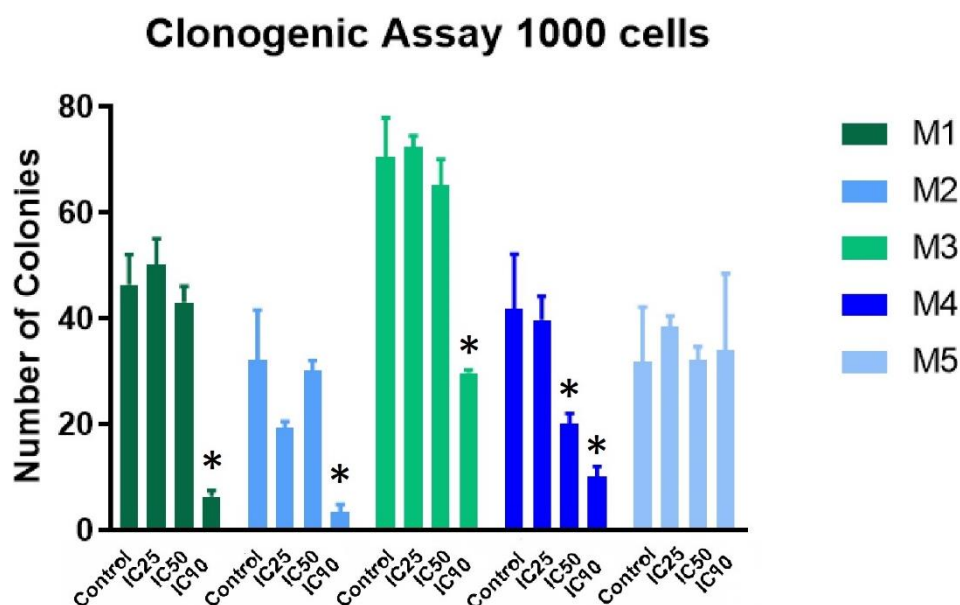


Figure 4.10- Quantification of clonogenic ability after treatment: The Y-axis shows number of colonies formed after 72 hours, while the X-axis shows the different treatments for all the 5 cell lines. The cells were treated with their IC₂₅, IC₅₀, IC₉₀ doses of cabozantinib. A two tailed students *t*-test were done to compare effects between treated and untreated cells. Abbreviations; * < 0,05. Mean +/- standard deviation (SD), n=3.

Figure 4.9 and figure 4.10 shows how the cell lines responded in their ability to make colonies after treatment with cabozantinib. All cell lines except the M5 cell line responded significantly after treatment with the IC₉₀ doses. When treated with this dose, the cells were not able to make more than 10 colonies. The M2 cell line showed some reduction in colony formation after treatment with the IC₂₅ dose, however this was not statistically significant. The M4 cell line was the most sensitive cell line for cabozantinib in this assay, and treatment with the IC₅₀ dose and the IC₉₀ dose significantly reduced the number of colonies. The M5 cell line responded poorly, with no significant effect from treatments. No difference in colony size was observed after treatment for the cell lines.

4.5 Spheroid experiments

Tumour spheroid observations

The spheroids were observed for 21 days to study the effect of cabozantinib on spheroid growth. A selection of representative images from each cell line are presented in figure 4.11-4.15, as well as the area of spheroids.

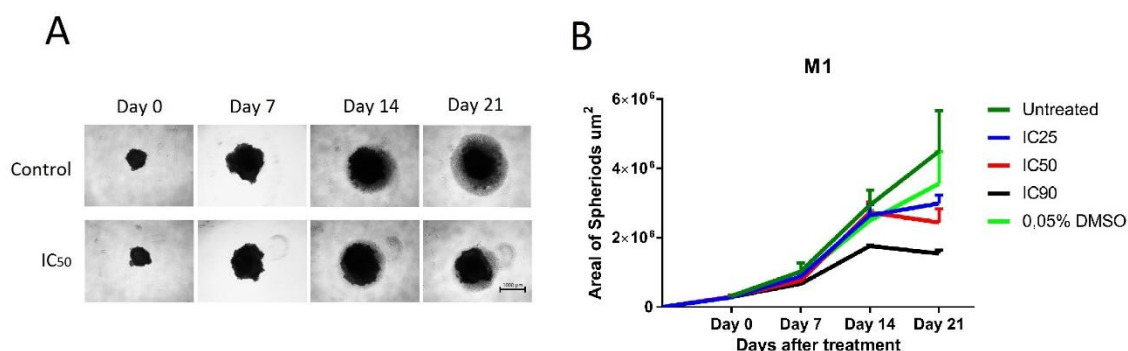


Figure 4.11- M1 spheroid growth during 21 days: Untreated and treated spheroids derived from the M1 cell line were followed for 21 days. Pictures were obtained at day 0, 7, 14, and 21, and the spheroid area were determined. (A) All pictures were obtained with a light microscope using the 4X objective. Scalebar = 1000 μm . (B) Spheroid area growth of untreated spheroids, and spheroids treated with IC₂₅, IC₅₀, IC₉₀ of cabozantinib or 0.05% DMSO. Abbreviations; Mean +/- standard deviation (SD), n=3.

The growth rate of M1 spheroids were not affected by treatment until day 7. After this time-point, a dose dependent growth inhibition could be seen until day 21, when the experiment was terminated. Significant effect was observed at day 21 for the IC₅₀ and IC₉₀ treatments, see table 4.2. These doses made the spheroids shrink from day 14 to 21, indicating that treatment may need some weeks to have effect.

Treatment with 0.05 % DMSO did not affect the spheroid growth, compared to untreated cells ($p = 0.14$).

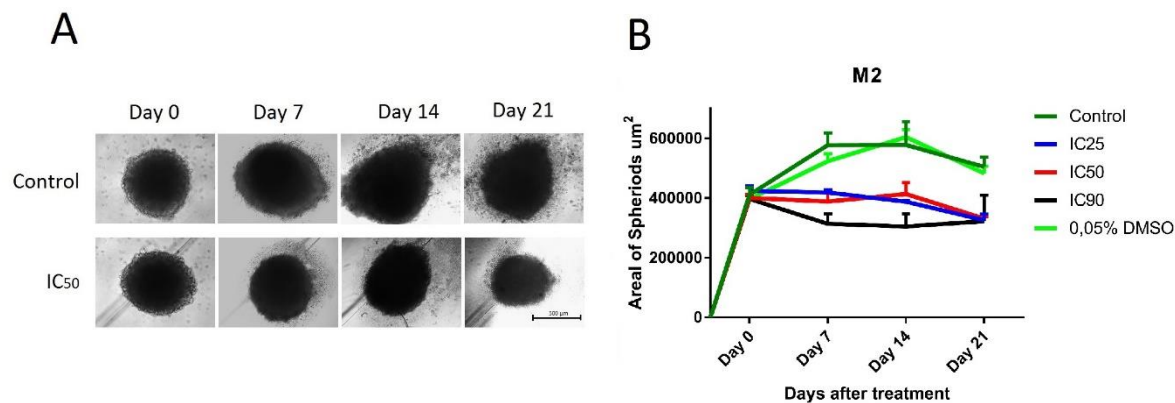


Figure 4.12- M2 spheroid growth during 21 days: Untreated and treated spheroids derived from the M2 cell line were followed for 21 days. Pictures were obtained at day 0, 7, 14, and 21, and the spheroid area were determined. (A) All pictures were obtained with a light microscope using the 10X objective. Scalebar = 1000 μm . (B) Spheroid area growth of untreated spheroids, and spheroids treated with IC₂₅, IC₅₀, IC₉₀ cabozantinib or 0.05% DMSO. Abbreviations; Mean \pm standard deviation (SD), n=3.

Figure 4.12 shows that spheroids derived from the M2 cell line had impaired growth ability after treatment with the IC₅₀ dose of cabozantinib. Control spheroids and spheroids treated with 0.05 % DMSO kept growing in the same rate until day 14, then the growth was reduced. This can be because spheroids reached their full size, based on available space left in the well. At day 21, all cabozantinib treated spheroid had almost equal areal size. A significant effect was seen for all treatments (table 4.2). As for the M1 spheroids, the M2 spheroids also decreased in size from day 14 to 21.

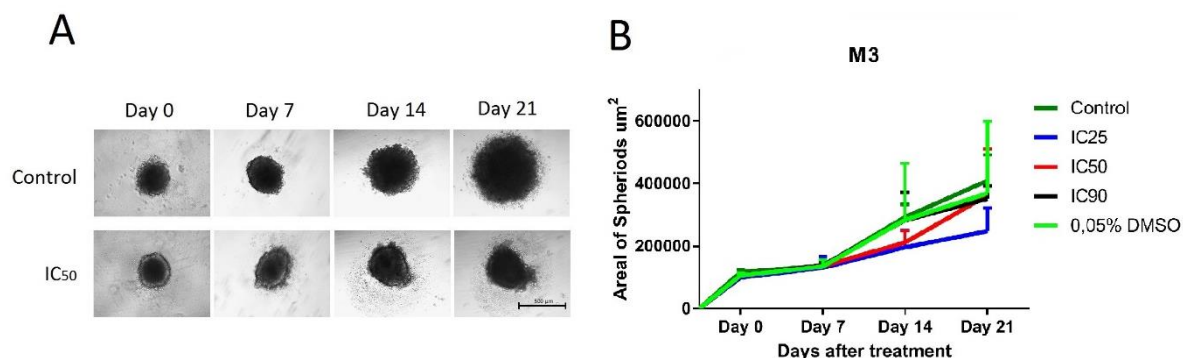


Figure 4.13- M3 spheroid growth during 21 days: Untreated and treated spheroids derived from the M3 cell line were followed for 21 days. Pictures were obtained at day 0, 7, 14, and 21, and the spheroid area were determined. (A) All pictures were obtained with a light microscope

using the 10X objective. Scalebar = 1000 μ m. (B) Spheroid area growth of untreated spheroids, and spheroids treated with IC₂₅, IC₅₀, IC₉₀ cabozantinib or 0.05% DMSO. Abbreviations; Mean +/- standard deviation (SD), n=3.

Figure 4.13-B shows that IC₂₅ treated M3 spheroids showed the largest inhibitory effect of the treatment. Although none of treatments exhibited significant effects, the pictures (A) shows that spheroids had growth difficulties after 14 days with treatment.

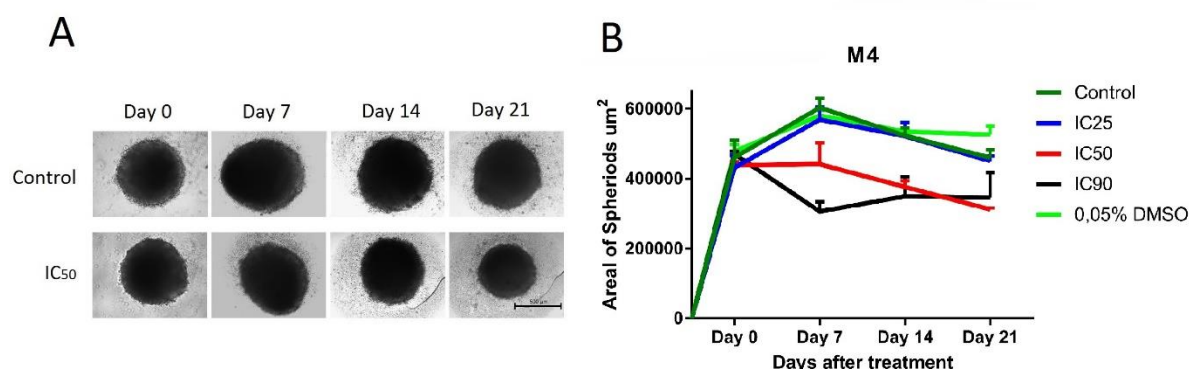


Figure 4.14- M4 spheroid growth during 21 days: Untreated and treated spheroids derived from the M4 cell line were followed for 21 days. Pictures were obtained at day 0, 7, 14, and 21, and the spheroid area were determined. (A) All pictures were obtained with a light microscope using the 10X objective. Scalebar = 1000 μ m. (B) Spheroid area growth of untreated spheroids, and spheroids treated with IC₂₅, IC₅₀, IC₉₀ cabozantinib or 0.05% DMSO. Abbreviations; Mean +/- standard deviation (SD), n=3.

Figure 4.14 shows that the growth rate of spheroids was significantly reduced after treatment with IC₅₀ and IC₉₀ doses of cabozantinib. IC₂₅, 0.05 % DMSO and untreated spheroids had approximately the same growth curve. The IC₂₅ dose did not seem to be a high enough dose to reduce the growth rate significantly compared to control spheroids.

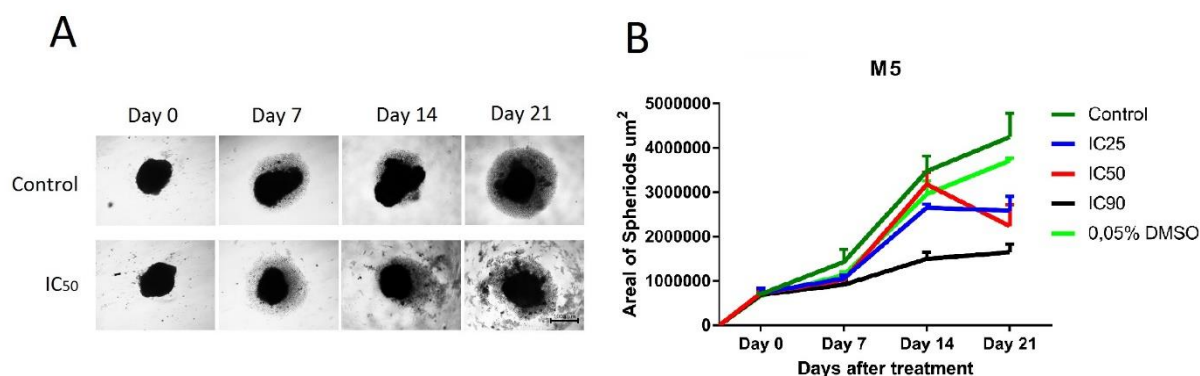


Figure 4.15- M5 spheroid growth during 21 days: Untreated and treated spheroids derived from the M5 cell line were followed for 21 days. Pictures were obtained at day 0, 7, 14, and 21, and the spheroid area were determined. (A) All pictures were obtained with a light microscope using the 4X objective. Scalebar = 1000 μ m. (B) Spheroid area growth of untreated spheroids, and spheroids treated with IC₂₅, IC₅₀, IC₉₀ cabozantinib or 0.05% DMSO. Abbreviations; Mean \pm standard deviation (SD), n=3.

Figure 4.15-A shows that spheroids had a poor capability to grow after treatment with the IC₅₀ dose of cabozantinib. From figure 4.15-B a dose dependent growth inhibition at day 21 was observed. 0.05 % DMSO and control spheroids kept growing in the same rate.

A two-tailed student t-test was done to compare the different treatments with the control samples. The calculated significance levels of treatments are presented in table 4.2.

Table 4.2: Significance levels, calculated comparing control spheroid area to the areas after different treatments of cabozantinib at day 7, 14 and 21. A two-tailed student *t*-test was used for these calculations. There was no significant difference between untreated control spheroids and spheroids treated with 0.05 % DMSO (not shown). Abbreviations; * <0.01 ** <0.001, ns. = not significant, n=3.

	Day 7			Day 14			Day 21		
	Control vs. IC ₂₅	Control vs IC ₅₀	Control vs. IC ₉₀	Control vs IC ₂₅	Control vs IC ₅₀	Control vs IC ₉₀	Control vs IC ₂₅	Control vs IC ₅₀	Control vs IC ₉₀
M1	ns.	ns.	ns.	ns.	ns.	*	ns.	*	*
M2	*	*	**	*	*	**	*	*	*
M3	ns.	ns.	ns.	ns.	ns.	ns.	ns.	ns.	ns.
M4	ns.	*	**	ns.	**	**	ns.	*	**
M5	ns.	ns.	*	*	ns.	**	*	*	**

Spheroids derived from the M2 cell line responded significantly for all treatments with cabozantinib, from day 7 to day 21. The effect was varying for the remaining cell lines, but in general significance was obtained for all IC₅₀ and IC₉₀ treatments at day 21. The exception was spheroids derived from the M3 cell line, which exhibited no significant effect throughout the experiment.

Migration assay

A migration assay was done to study the effect of cabozantinib on cell outgrowth and migration from spheroids. The spheroids were treated with IC₂₅, IC₅₀, or IC₉₀ doses of cabozantinib, and the cell outgrowth and migration was measured at day 0, 2, 3 and 4. The

M1 spheroids were not able to attach to collagen, and thus cell migration could not be studied.

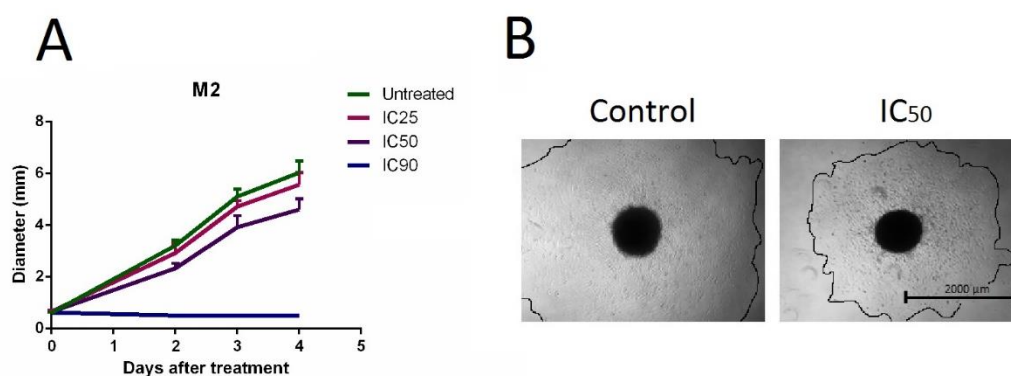


Figure 4.16-migration of M2: A: The diameter of migrated area is presented. B: Representative pictures of outgrowth from an untreated spheroid (control) and a spheroid treated with the IC₅₀ dose. Abbreviations; Mean +/- standard deviation (SD), n=3.

Treatment with IC₉₀ inhibited all growth and migration of the M2 cell line (Figure 4.17). Cell migration from the spheroids still occurred during treatment with the IC₅₀ doses, but in a considerably lower rate compared to control cells (table 4.3).

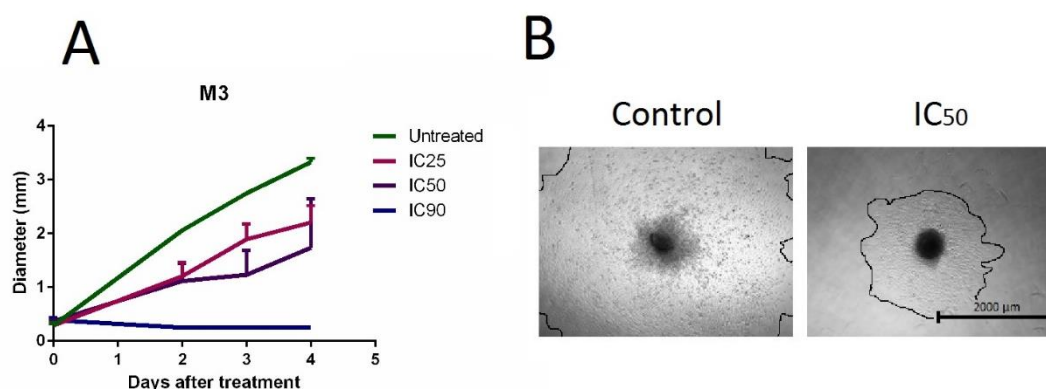


Figure 4.17-migration of M3: A: The diameter of migrated area is presented. B: Representative pictures of outgrowth from an untreated spheroid (control) and a spheroid treated with the IC₅₀ dose. Abbreviations; Mean +/- standard deviation (SD), n=3.

Also for the M3 spheroids, there was a significant dose-dependent inhibition in cell migration from the spheroids (figure 4.17 and table 4.3). The IC₉₀ dose completely abrogated cell migration.

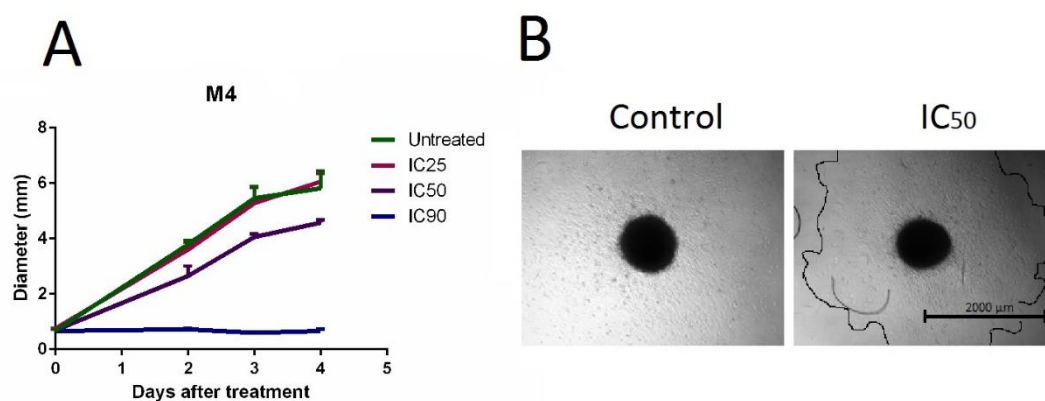


Figure 4.18-migration of M4: A: The diameter of migrated area is presented. B: Representative pictures of outgrowth from an untreated spheroid (control) and a spheroid treated with the IC₅₀ dose. Abbreviations; Mean +/- standard deviation (SD), n=3.

For the M4 and M5 cell line, treatment with the IC₂₅ dose did not affect cell migration. However, after treatment with the IC₉₀ and IC₅₀ doses, a dose significant inhibition was observed. (figure 4.19 and 4.20)

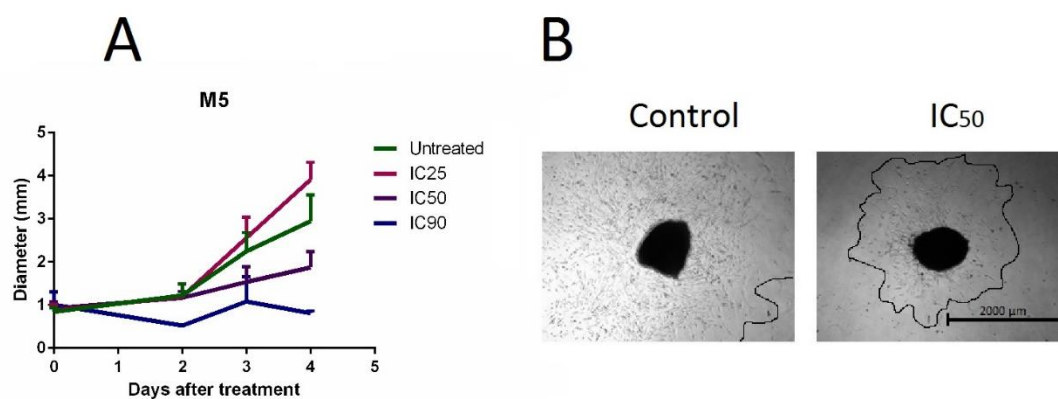


Figure 4.19-migration of M5: A: The diameter of migrated area is presented. B: Representative pictures of outgrowth from an untreated spheroid (control) and a spheroid treated with the IC₅₀ dose. Abbreviations; Mean +/- standard deviation (SD), n=3.

Table 4.3: Calculation of significant difference in cellular outgrowth from treated spheroids, compared to outgrowth from untreated spheroid at day 4. A two-tailed students *t*-test was used for these calculations. Aberrations; * < 0.01, **< 0.001, ***< 0.0001, ns. = not significant, n=3.

Significance level at day 4			
	Control vs. IC ₂₅	Control vs. IC ₅₀	Control vs. IC ₉₀
M2	ns.	**	***
M3	**	**	**
M4	ns.	*	**
M5	ns.	*	*

Cellular outgrowth from the M3 spheroids was significantly inhibited for all doses of cabozantinib (table 4.3). The statistical testing showed that there were no differences in cellular migration when treating the M2, M4 and M5 spheroids with the IC₂₅ doses, however for the two higher doses the migration was significantly inhibited.

Confocal microscopy of live/dead stained spheroids

Spheroids were stained with the live/dead kit (Molecular Probes) to study whether the spheroids contained dead cells, or if the dead cells were continuously washed out from the spheroids. In this experiment, untreated control spheroids and IC₅₀ treated spheroids were used. Due to time limits, this experiment was only performed on the M4 cell line. This cell line was chosen due to its great ability to form spheroids.

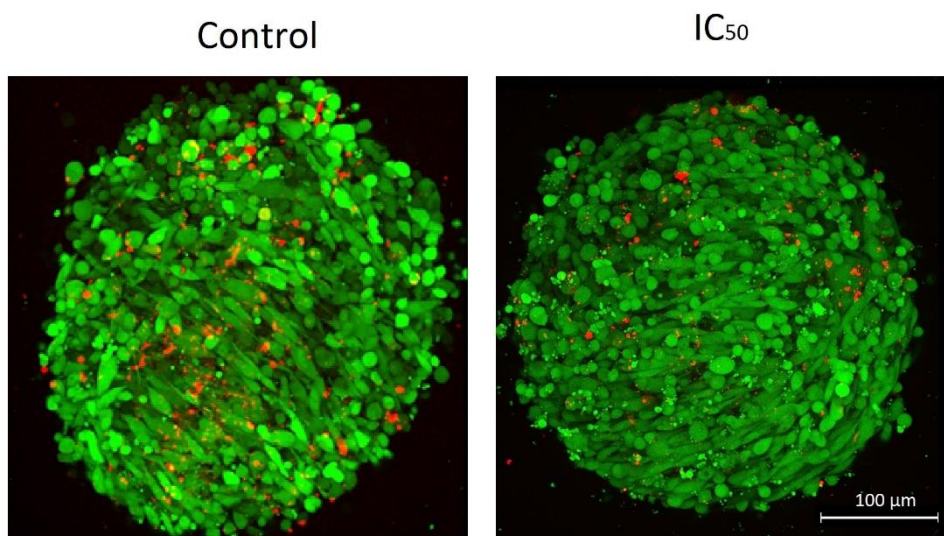


Figure 4.20- live/ dead staining of spheroids: untreated (control) and IC₅₀ cabozantinib treated spheroids made from the M4 cell line. The spheroids were grown for 7 days, and treated for 72 hours before images were obtained. Cells are stained with live/dead kit (Molecular Probes). Calcein AM stains living cells with green fluorescent and ethidium homodimer-1 stains dead cells red.

Figure 4.16 shows how spheroids from the M4 cell line respond to treatment with IC₅₀ dose of cabozantinib. There were no apparent differences in the number of dead cells or a size difference in treated and untreated spheroids.

4.6 Western blots

Detection of p-KIT, p-MET and p-VEGFR2 was done by western blot. GAPDH was used as a loading control. The western blots of p-VEGFR2 resulted in many unspecific bands, making the interpretations ambiguous. Since p-VEGFR2 is a high molecular antibody (230 kD), it was obvious that a considerable protocol optimization was needed to get reliable results when using canine cell lines. This was not done, due to time limitations in this thesis.

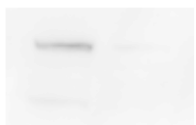













	M1		M2		M3		M4		M5	
	C	IC50	C	IC50	C	IC50	C	IC50	C	IC50
p-KIT										
p-MET	No bonds									
GAPDH										

Figure 4.21- Western blots. Detection of p-KIT and p-MET. GAPDH was used as loading control.

Figure 4.21 shows that p-KIT was decreased after treatment with cabozantinib, as was also expected. No bond was detected for p-MET for the M1 cell line. For the other cell lines, p-MET was not decreased after IC₅₀ treatment with cabozantinib. For the M3 cell line it seemed that p-MET was increased after treatment, which was unexpected. GAPDH was detected for all cell lines in a stable amount.

5. Discussion

Generally, OM is associated with a poor prognosis, both for humans and dogs. Current treatment strategies are not effective, and high metastasis rates combined with local recurrence are the main causes of death [1, 11, 13]. Cabozantinib is recently FDA approved as a treatment against advanced renal cell carcinoma and metastatic medullary thyroid cancer, and several preclinical studies have shown effects on different cancer types [50, 54].

In this project, a variety of *in vitro* assays with cabozantinib were used to evaluate its anticancer effect against canine OM cell lines. Western blots were used to evaluate if cabozantinib had the potential of inhibiting cancer related RTKs.

5.1 Cell viability assays

First, a resazurin assay was performed to measure cell viability. All cell lines responded, a dose-dependent effect of cabozantinib was observed, and the calculated IC_{50} doses were in the low μM range.

A similar effect has been seen in the literature. Zhang and colleagues measured decreased cell viability in neuroblastoma cell lines (BxPc-3, MIA-paCa2, Capan-1 and CRL-4023) after treatment with cabozantinib [95]. Furthermore, Hage and coworkers showed that pancreatic ductal adenocarcinoma cell lines (SK-N-BE(2), CHP 212, LAN5, CHLA-20, SK-N-D2, SK-N-SH, SH-SY5Y, NGP, LA155N, IMR-31 and CHP-134) also exhibited reduced viability when treated with 5-10 μM of cabozantinib [96]. Both studies used treatment concentrations close to the IC_{50} doses calculated in this thesis.

The results from the resazurin assay lay the foundation for further experiments with cabozantinib, as the IC_{25} , IC_{50} and IC_{90} doses was calculated and used as treatment doses in further assays.

The resazurin assay is a reliable method to measure viable cells. The dye measure reduction of resazurin into resorufin, which is in direct correlation to the number of viable cells in the wells [78]. Normally, 4 hours is sufficient to measure signal above background, but the incubation time is dependent on the metabolic activity of the cells, which can differ between cell type, cell density and growth medium [97]. The cell lines used in this thesis had a high metabolism, and incubation with 4 hours was sufficient to show that cabozantinib did inhibit tumour growth. As mentioned, the IC₅₀ doses used in this thesis corresponded to IC₅₀ cabozantinib doses reported in the literature, and the viability pictures confirmed the resazurin assay results, which substantiate the viability results.

Cell lines cultured in monolayers can suffer from limitations concerning drug sensitivity. Studies have shown that 3D *in vitro* culture systems present a better model concerning drug sensitivity [98, 99]. An example is where tumour spheroids derived from a breast cancer cell line (MDA-MB-231) exhibited a significant lower IC₅₀ to cisplatin when plated in 2D monolayer compared to 3D spheroids [100]. Cabozantinib doses used for the spheroid assays in this thesis might have been lower than if these were determined using a spheroid model vs. a monolayer model. Still, aggregated data from 3D assays demonstrated beneficial effect of treatment, giving a good indication of treatment response.

5.2 Apoptosis assay

The results from the annexin V assay demonstrated a dose-dependent effect of cabozantinib for the M1, M2 and M4 cell lines with increased percentages of apoptotic cells.

Hage and colleagues observed similar effect when pancreatic ductal adenocarcinoma cell lines (for cell line information, see section 5.1) were treated with low concentrations (5-10 µM) of cabozantinib [96]. In addition, Li and co-workers showed that oral squamous carcinoma cell lines (BHY and HSC-3) exhibited increasing annexin V staining with increasing doses of cabozantinib after 24 hours of treatment [101].

Furthermore, cabozantinib was also found to induce apoptosis *in vitro* and *in vivo* for multiple prostate cancer cell lines (Ace-1, C4-2B, and LuCaP 35) by Dai and collaborators [102]. The same effect was observed in colorectal cancer cell lines by Song and co-workers. *In vivo* results revealed a significant dose-dependent increase of apoptosis. They also observed an increase of cleaved caspase 3 after 3 days of treatment, which is associated with apoptosis [103]. These results show that cabozantinib can induce apoptosis *in vitro* as well as *in vivo* for several malignancies, making it likely to apply for human and canine OM as well.

Whereas for the M3 and M5 cell lines, the treatment was not as effective as for the remaining cell lines, and only the highest dose of cabozantinib induced apoptosis. The percentage of living cells were still high, and a significant effect was not obtained with IC₂₅ or IC₅₀ treatment. This suggests that IC₂₅ or IC₅₀ treatment with cabozantinib was not able to induce apoptosis in these cell lines, but sufficient to inhibit growth. Only the IC₉₀ dose of cabozantinib induced apoptosis and inhibited growth, indicating that these cell lines are not resistant to treatment, but need higher treatment doses than IC₅₀ to induce apoptosis.

Data from our tumour spheroid observation assays (see section 4.5) where growth area was measured during 21 days, support the apoptosis results. Growth of the IC₂₅ and IC₅₀ treated M3 spheroids and the IC₂₅ treated spheroids harvested from the M5 cell lines exhibited decreased spheroid size, but the spheroids did not shrink in size, as seen for the remaining cell lines. This indicates that apoptosis is not induced after treatment with low doses of cabozantinib for the M3 and M5 cell lines.

Lin and colleagues studied the effect of cabozantinib on normoxic and hypoxic medullary thyroid cancer cell lines. After cabozantinib treatment (50, 100, or 200 nM), they observed that treatment response was influenced by the oxygen status of the cells. Hypoxic cells exhibited significantly lower apoptosis rates compared with normoxic cells [104]. Information about cells oxygen level before and after treatment, as well as before apoptosis analyzation could be of value to understand why some cell lines responded to low doses of cabozantinib, and others not.

5.3 Cell cycle assay

Cabozantinib did not cause any changes in the cell cycle distribution for the M1, M3, M4 or M5 cell lines. This indicates that cabozantinib eradicates tumour cells by apoptosis rather than cell cycle arrest for the M1 and M4 cell lines. Only the M2 cell line was significantly arrested in the G0/G1 phase after IC₅₀ treatment of cabozantinib, raising the question of a dual eradication mechanism of cabozantinib, as this cell line responded significantly to both assays.

G0/G1 arrest is an effect of cabozantinib which is consistently seen throughout the literature. Ruan and co-workers treated papillary thyroid carcinoma cell lines (BHP 2-7) with 0.05 and 0.5 μ M cabozantinib for 24 hours, causing 81.3 % and 97.7 % G0/G1 arrest, respectively [105].

Li and co-workers, as well as Xiang and colleagues experienced G0/G1 arrest after treatment with low doses of cabozantinib on oral squamous cell carcinoma cell lines and hepatocellular carcinoma cell lines [101, 106]. Interestingly, they also detected a downregulation of cyclin A and cyclin D, which are important regulators for the cell cycle, enabling the cells to proceed to M phase and S phase, respectively. Cyclin B1, causing the cells to go from M phase to G0 phase, was also increased after cabozantinib treatment in the oral squamous cell carcinoma cell lines [101, 106].

As explained in section 1.3, overexpression of RAS and KIT mutations are common genetic alterations observed in canine OM. Figure 1.2 illustrates how these abnormalities can cause increased cyclin D. As shown in figure 4.18, p-KIT was downregulated in all cell lines, but if a RAS mutation is present, the cells may still be able to continue the production of cyclin D.

A G0/G1 arrest was not seen for all cell lines in this study, and a further examination of cyclin expression or RAS mutation status was not done, due to time limitations. To understand why cabozantinib did not affect the cell cycle distribution, information about expressed cyclins after treatment, as well as RAS mutation status could have been valuable.

5.4 Clonogenic assay

Li and colleagues proved that low doses of cabozantinib reduced the potential of human oral squamous cell carcinoma cell lines (BHY and HSC-3) to form colonies. The cell lines were treated with 0.3, 0.6 and 1.2 μM of cabozantinib, which is lower than the IC_{50} doses used in this thesis [101]. Still, a poor effect on reducing tumour clonogenicity was seen in our work, except for the M4 cell line. In this cell line, a dose dependent inhibition was seen. For the remaining cell lines, the highest dose (100 μM) showed significant effects except for the M5 cell line, which responded poorly to all treatments.

It is known that β -catenin, the main effector of the canonical Wnt pathway is involved in clonogenic growth of various malignancies [107, 108]. In our work, all our cell lines have inactive canonical Wnt pathways [88], thus this is likely not the explanation for the results. Changes in β -catenin after treatment was therefore not studied in this thesis.

The AKT pathway, when exhibiting an active mTOR, is also important for clonogenicity. Kent and co-workers showed that inhibition of mTOR in malignant canine melanoma strongly decreased colony formation [109]. The activation of the AKT/mTOR signaling pathway is important in the development of melanoma in humans and dogs. This pathway can also be activated by inactivation mutations or a complete loss of the PTEN tumour suppressor gene, which has been detected in some oral melanomas in dogs [28]. PTEN is an inhibitor of the PI3K pathway, and when inactivated, growth and survival of the cell will be induced. mTOR activation was found in 100 % of 43 dogs with mucosal melanoma by Wei and colleagues, including the cell lines used in this work [89]. If there is a mutation in the signal proteins, like in PTEN, AKT or mTOR keeping the PI3K pathway active, cabozantinib will likely not be able to inactivate the pathway.

Mapping these mutations for the cell lines used in this thesis might be useful to do in further studies of cabozantinib.

5.5 Spheroid experiments

Tumour spheroid observation

Cabozantinib reduced spheroid growth and spheroid formation in a dose-dependent manner for all cell lines. For the M1, M2 and M4 cell lines, treatment caused spheroids to shrink in size. Some control spheroids stopped growing because of lack of space. If repeated, smaller spheroids should have been used. Due to time limits, this assay was not repeated. Even though some control spheroids stopped growing, significant effects were seen.

A dose dependent effect of cabozantinib on spheroid size was also seen by Hage and co-workers. They treated pancreatic ductal adenocarcinoma cell lines with 5, 7.5 and 10 μM cabozantinib for 14 days [96].

A major problem with cancer treatment is the development of resistance to treatment. A large population of cells die upon chemotherapy, but if a small population is resistant to the drug, so called “cancer stem like cells” survive, they will get more enriched by every cell cycle [110]. Long-term treatment with cabozantinib is therefore of great interest. Hage and co-workers showed that long-term treatment with cabozantinib may cause changes in expression of pro- and anti-apoptotic molecules. After treatment with 5-6 μM of cabozantinib followed by 2 weeks of recovery, surviving cells were further studied. Results showed upregulated expression of pro-apoptotic markers (e.g. cleaved Caspase-3, TRAIL R2, FAS) as well as for some anti-apoptotic markers (e.g. Bcl-2, IAP-1, Survivin and XIAP). They also showed that the pro-apoptotic proteins Bim and p53 were downregulated. Further, SOX2 were downregulated, suggesting lower self-renewal potential. Both pro- and anti-cancer proteins were changed after long-term treatment with cabozantinib, indicating a slight increase in resistance to long-term repeated treatment with cabozantinib [96]. However, unpublished data from our laboratory on long-term cabozantinib treatment of glioblastoma cell lines suggests that resistance to treatment does not occur.

Liu and colleagues have studied the effect of cabozantinib on “cancer stem like cells” *in vivo*. Stromal cells were treated with 10 μM cabozantinib for 24 hours before transplanted in

fertilized eggs. Cabozantinib inhibited growth and induced severe developmental defects in the chicken embryos. The study suggests that cabozantinib overcome the “cancer stem like cell” signaling, because stem cell and developmental signaling is strongly related [111].

Long-term treatment with cabozantinib for OM has not been evaluated in the literature, but should be assessed when studying cabozantinib and OM further.

Migration assay

In this thesis IC₅₀ and IC₉₀ doses of cabozantinib reduced migration significantly ($p < 0,01$) *in vitro* for all cell lines. Navis and colleagues observed the same effect when studying human glioblastoma cell lines (E98) [112]. In addition, *in vivo* studies with cabozantinib has shown significant reduction of metastasis, angiogenesis and tumour growth for different malignancies [49, 106]. This makes cabozantinib a promising agent to reduce migration and metastasis for OM, as well as other malignancies.

Confocal microscopy of Live/Dead stained spheroids

Pictures of IC₅₀ treated and untreated spheroids was obtained for the M4 cell line. Number of dead and live cells seemed to be equal for both treated and untreated spheroids. No morphologic changes were seen.

Data from the tumour spheroid observation assay (see figure 4.14), showed that spheroid size was affected after 7 days of treatment, and the antitumour effect was seen throughout the 21 days of observation. Images obtained with confocal microscopy was treated for 72 hours, suggesting that longer treatment is needed to see the same effect seen in the tumour spheroid observation assay.

As seen in the viability images (see section 5.1) few red fluorescent cells were seen. This can be explained by the fact that dead cells on the outside of the spheroid continually is washed out, thus not imaged.

5.6 Western blots

The MET receptor is important in tumour signaling, and is implicated in migration and embryogenesis. Together with VEGFR which induces angiogenesis, these receptors are important in the inhibition of cell migration. Treatment with VEGFR inhibitors alone in preclinical trials have shown to increase the metastasis rate and invasiveness. Increased expression of c-MET is also believed to be a consequence of treatment, due to hypoxia induced activation of MET [103, 113, 114]. KIT is often implicated in OM, and treatment targeting only KIT have showed to activate MET in some malignancies [75]. Triple inhibition of these RTKs is believed to solve the cross signaling between these pathways. Cabozantinib has potential to inhibit all three receptors, making it able to reduce and inhibit cell migration and growth *in vitro*, and metastasis, angiogenesis and tumour growth *in vivo*.

For cabozantinib to have anticancer effects, the targeted RTKs must be sufficiently inhibited, making them unable to get into their active phosphorylated form. p-VEGFR, p-KIT and p-MET was therefore studied by western blots.

The amount of p-KIT was detected in a stable amount in the control samples. In IC₅₀ treated samples the protein level was decreased or not present. These results indicate that cabozantinib effectively inhibits the KIT receptors in these cell lines.

Equivalent results have been shown in the literature. Yakes and colleagues showed that 7.8 µmol/L cabozantinib strongly inhibited phosphorylation of KIT *in vivo* after injection of cell lines from different malignancies (A431, B16F10, C6, H441, H69, Hs746T, HT1080, MS1, PC3, SNU-1, SNU-5, SNU-16, U87MG and MDA-MB-231) in mice [49]. Cohen and co-workers did a study on mice where gastrointestinal stromal tumour cells had been injected. After 8 weeks of treatment with 60 mg/kg of cabozantinib, histological samples showed no

sign of KIT staining. They also showed that cabozantinib had a higher antitumour effect than imatinib (RTK inhibitor targeting KIT [115]), both for imatinib sensitive and resistant models [75]. This is relevant because targeting only KIT can activate MET in some malignancies, dual targeting of both receptors with cabozantinib have been proven to be more effective [75].

In this thesis, no consistent difference in p-MET amount was seen before or after treatment. Still, an antitumour effect was seen after cabozantinib treatment.

In a study by Yakes and colleagues, rats with H441 tumours were treated with an oral dose of 100 mg/kg cabozantinib before p-MET were investigated. They showed that p-MET levels were downregulated 2-8 hours after treatment, but after 48 hours p-MET returned to basal levels. Still, cabozantinib inhibited tumour growth significantly *in vivo* [49]. In our work, cells were treated for 72 hours, which may have been enough time for p-MET to return to basal levels, like seen in Yakes study. For further investigation, western blots of p-MET after 2 and 8 hours should be performed to supplement this hypothesis.

Another reason for our results could be that cabozantinib is not able to inhibit the MET receptor in canine cells, because of potential differences between the human and canine MET protein structure. As of today, no data about this subject could be found in the literature. However, xenograft *in vivo* studies with rats and mice have shown effects of cabozantinib, making it likely that cabozantinib would inhibit RTKs in canines as well.

Yet another explanation could be that the apoptotic and dead cells floating in the medium were removed during cell lysate preparations. These cells might have died because of RTK inhibition, including MET inhibition. Therefore, a western blot on the apoptotic cells might have shown decreased levels of p-MET.

The MET receptor seemed to be unaffected by cabozantinib, but still beneficial effect of cabozantinib was seen in our assays. This can imply that inhibition of KIT, in addition to RTKs not investigated in this study is sufficient to reduce tumour progression in canine OM

cell lines. Cabozantinib can inhibit several RTKs, and may have inhibited others than which have been evaluated in this thesis, contributing to decreased tumour progression and growth.

5.7 Concluding remarks

This thesis has used fundamental *in vitro* assays with canine OM cell lines to study cabozantinib as a treatment opportunity for OM. In accordance with the literature, cabozantinib did decrease cell viability in a dose-dependent manner for all 5 cell lines [95, 96]. In consistency with the literature, cabozantinib significantly induced apoptosis for all cell lines [96, 101-103]. However, for the M3 and M5 cell line, this effect was only seen after treatment with the IC₉₀ (100 µM) treatment. For the remaining cell lines, a dose-dependent effect was observed, with increasing number of apoptotic cells.

Cell cycle distribution was in general not affected by treatment, although one cell line (M2) showed a significant G0/G1 arrest. Arrest in the G0/G1 phase is a consistent finding in the literature [101, 105, 106], raising the question of a dual tumour prevention mechanism through both inducing apoptosis and cell cycle arrest.

The M3 and M5 cell line did not respond by inducing apoptosis or G0/G1 arrest after low treatment doses of cabozantinib. This indicates that low doses of cabozantinib only reduce growth and migration *in vitro* for these cell lines.

Cabozantinib did not influence the clonogenic potential of the cells after using the lowest doses, but decreased colony formation after treatment with the IC₉₀ (100 µM) dose.

In general, the results from the spheroid assays exhibited better effect of treatment than the monolayer assays. Growth inhibition and decrease in size of spheroids were observed, as well as inhibition of cell outgrowth and migration from spheroids. These are important findings, as 3D models are believed to be clinically more relevant. The results in this thesis

indicate that cabozantinib may have anticancer effect also on OM in an *in vivo* setting [98, 99].

Cabozantinib did not influence p-MET levels after 72 hours. These results do not exclude that levels were affected during the 72 hours of treatment, as Yakes and co-workers have revealed that p-MET levels can be downregulated after cabozantinib treatment before returning to basal levels within 24 hours after treatment [49]. Changes in phosphorylated protein levels over time was not studied in this thesis.

p-KIT levels were downregulated or not present after cabozantinib treatment for all cell lines. The results indicate that inhibition of this receptor may be enough to decrease tumour progression and growth *in vitro*. Because this study only explored the effect of cabozantinib on the KIT and MET pathways, the results in this thesis do not exclude the possibility that cabozantinib blocks other pathways as well, resulting in the antitumour behavior seen.

5.8 Future aspects

The assays should be repeated with expanded treatment doses. The concentration range between the IC₅₀ and IC₉₀ doses used in this work were extensive. Expanded treatment concentrations to fill this gap, would be favourable to establish the minimum dose of response, which likely lies between IC₅₀ and IC₉₀.

As the cell lines responded differently to the different assays, the experiments should be repeated on more OM cell lines, including OM cell lines from humans, to see if the same trend can be observed.

Information on protein level expression in these OM cell lines are available (table 3.2). Still, this should be further explored, by expanding on the western blot assay to further map the genetic alterations that may have importance for OM progression. This could lead to an

improved understanding of which signalling pathways are more important in the progression of canine OM, and these data could then be further explored clinically.

Low doses of cabozantinib induced apoptosis for some cell lines, and induced G0/G1 arrest in one cell line. However, the data shown in this study did not coincide completely with what has been published previously in the literature, and should therefore be expanded upon. It should be emphasized that this work studied apoptosis and cell cycle after only 72 hours of treatment. These assays should therefore be repeated, including several time intervals between 2-72 hours.

Protein studies of expanded RTKs should be done to understand which RTKs are targeted in OM cell lines during cabozantinib treatment, as cabozantinib can block several tumour associated RTKs. Also, long-term treatment should be studied further, as a frequent problem with drug therapies is the development of resistance.

Cultured cells resemble the parent tumour to a certain degree, but after several passages cells commonly change their phenotype, and the growth environment can influence growth and tumour characteristics. To validate the findings in this thesis, *in vivo* preclinical studies of cabozantinib should therefore be performed. If successful, animal trials and human trials will further reveal if cabozantinib can be effective as a treatment of OM.

It is not unlikely that Cabozantinib might have synergistic effects if combined with other drugs, such as for instance immunotherapies. Exelixis has in cooperation with Bristol-Myers Squibb Company and Roche ongoing clinical trials, where cabozantinib is combined with immunotherapy to increase the efficiency of treatment [116].

References

1. Hicks, M.J. and C.M. Flaitz, *Oral mucosal melanoma: epidemiology and pathobiology*. Oral Oncology, 2000. **36**(2): p. 152-69.
2. Barker, B.F., et al., *Oral mucosal melanomas: the WESTOP Banff workshop proceedings*. Western Society of Teachers of Oral Pathology. Oral Surgery, Oral Medicine, Oral Pathology, Oral Radiology, and Endodontology, 1997. **83**(6): p. 672-9.
3. Moore, E.S. and H. Martin, *Melanoma of the upper respiratory tract and oral cavity*. Cancer, 1955. **8**(6): p. 1167-76.
4. Meleti, M., et al., *Oral malignant melanoma: A review of the literature*. Oral Oncology, 2007. **43**(2): p. 116-121.
5. Ebenezer, J., *Malignant melanoma of the oral cavity*. Indian Journal of Dental Research, 2006. **17**(2): p. 94-6.
6. Luna-Ortiz, K., et al., *Comparative study between two different staging systems (AJCC TNM VS BALLANTYNE'S) for mucosal melanomas of the Head & Neck*. Medicina Oral, Patología Oral y Cirugía Bucal, 2016. **21**(4): p. e425-30.
7. Adisa, A.O., W.O. Olawole, and O.F. Sigbeku, *Oral amelanotic melanoma*. Annals of Ibadan Postgraduate Medicine, 2012. **10**(1): p. 6-8.
8. Tlholoe, M.M., et al., *Oral mucosal melanoma: some pathobiological considerations and an illustrative report of a case*. Head and Neck Pathology, 2015. **9**(1): p. 127-34.
9. McLean, N., M. Tighiouart, and S. Muller, *Primary mucosal melanoma of the head and neck. Comparison of clinical presentation and histopathologic features of oral and sinonasal melanoma*. Oral Oncology, 2008. **44**(11): p. 1039-1046.
10. Patel, S.G., et al., *Primary mucosal malignant melanoma of the head and neck*. Head Neck, 2002. **24**(3): p. 247-57.
11. Dank, G., et al., *Use of adjuvant carboplatin for treatment of dogs with oral malignant melanoma following surgical excision*. Veterinary and Comparative Oncology, 2014. **12**(1): p. 78-84.
12. Bergman, P.J., *Canine oral melanoma*. Clinical Techniques in Small Animal Practice, 2007. **22**(2): p. 55-60.
13. Treggiari, E., J.P. Grant, and S.M. North, *A retrospective review of outcome and survival following surgery and adjuvant xenogeneic DNA vaccination in 32 dogs with oral malignant melanoma*. Journal of Veterinary Medical Science, 2016. **78**(5): p. 845-50.

14. Chang, A.E., L.H. Karnell, and H.R. Menck, *The National Cancer Data Base report on cutaneous and noncutaneous melanoma: a summary of 84,836 cases from the past decade. The American College of Surgeons Commission on Cancer and the American Cancer Society*. Cancer, 1998. **83**(8): p. 1664-78.
15. Jay Harvey, H., *Oral Tumors*. Veterinary Clinics of North America: Small Animal Practice, 1985. **15**(3): p. 493-500.
16. Statistisk Sentralbyrå. *Kjæledyr i norske husholdninger*. 1994; Available from: <https://www.ssb.no/befolkning/artikler-og-publikasjoner/kjaeledyr-i-norske-husholdninger>.
17. MacEwen, E.G., *Spontaneous tumors in dogs and cats: models for the study of cancer biology and treatment*. Cancer and Metastasis Reviews, 1990. **9**(2): p. 125-136.
18. Doll, R., *Strategy for detection of cancer hazards to man*. 1977.
19. Vail, D.M. and E.G. Macewen, *Spontaneously occurring tumors of companion animals as models for human cancer*. Cancer investigation, 2000. **18**(8): p. 781-792.
20. Moore, A.S., et al., *Preclinical study of sequential tumor necrosis factor and interleukin 2 in the treatment of spontaneous canine neoplasms*. Cancer Research, 1991. **51**(1): p. 233-8.
21. Rapidis, A.D., et al., *Primary malignant melanoma of the oral mucosa*. Journal of Oral and Maxillofacial Surgery, 2003. **61**(10): p. 1132-9.
22. Curtin, J.A., et al., *Somatic activation of KIT in distinct subtypes of melanoma*. Journal of Clinical Oncology, 2006. **24**(26): p. 4340-6.
23. Rivera, R.S., et al., *C-kit protein expression correlated with activating mutations in KIT gene in oral mucosal melanoma*. Virchows Archiv, 2008. **452**(1): p. 27-32.
24. Buery, R.R., et al., *NRAS and BRAF mutation frequency in primary oral mucosal melanoma*. Oncology reports, 2011. **26**(4): p. 783.
25. Tacastacas, J.D., et al., *Update on primary mucosal melanoma*. Journal of the American Academy of Dermatology, 2014. **71**(2): p. 366-375.
26. Pollock, P.M. and P.S. Meltzer, *A genome-based strategy uncovers frequent BRAF mutations in melanoma*. Cancer Cell, 2002. **2**(1): p. 5-7.
27. Edwards, R., et al., *Absence of BRAF mutations in UV-protected mucosal melanomas*. Journal of medical genetics, 2004. **41**(4): p. 270-272.
28. Koenig, A., et al., *Expression and significance of p53, rb, p21/waf-1, p16/ink-4a, and PTEN tumor suppressors in canine melanoma*. Veterinary Pathology, 2002. **39**(4): p. 458-72.
29. Cláudia Malheiros Coutinho-Camillo, S.V.L., Fernando Augusto Soares. *Head and Neck: Primary oral mucosal melanoma* 2015; Available from: <http://atlasgeneticsoncology.org/Tumors/OralMelanomaID6647.html>.

30. Helsedirektoratet. *Nasjonalt handlingsprogram med retningslinjer for diagnostikk, behandling og oppfølging av maligne melanomer*. 2016; Available from: <https://helsedirektoratet.no/Lists/Publikasjoner/Attachments/1222/IS-2489-Handlingsprogram-maligne-melanomer-5.utgave.pdf>.
31. Edge, S.B. and C.C. Compton, *The American Joint Committee on Cancer: the 7th edition of the AJCC cancer staging manual and the future of TNM*. Annals of Surgical Oncology, 2010. **17**(6): p. 1471-4.
32. Warszawik-Hendzel, O., et al., *Melanoma of the oral cavity: pathogenesis, dermoscopy, clinical features, staging and management*. Journal of Dermatological Case Reports, 2014. **8**(3): p. 60-6.
33. Kingdom, T.T. and M.J. Kaplan, *Mucosal melanoma of the nasal cavity and paranasal sinuses*. Head Neck, 1995. **17**(3): p. 184-9.
34. Eggermont, A.M.M., et al., *Utility of adjuvant systemic therapy in melanoma*. Annals of Oncology, 2009. **20**(Suppl 6): p. vi30-vi34.
35. MacEwen, E.G., et al., *Canine oral melanoma: comparison of surgery versus surgery plus Corynebacterium parvum*. Cancer Investigation, 1986. **4**(5): p. 397-402.
36. Yi, J.H., et al., *Dacarbazine-based chemotherapy as first-line treatment in noncutaneous metastatic melanoma: multicenter, retrospective analysis in Asia*. Melanoma research, 2011. **21**(3): p. 223-227.
37. Piras, L.A., et al., *Prolongation of survival of dogs with oral malignant melanoma treated by en bloc surgical resection and adjuvant CSPG4-antigen electrovaccination*. Veterinary and Comparative Oncology, 2016.
38. Ramos-Vara, J., et al., *Retrospective study of 338 canine oral melanomas with clinical, histologic, and immunohistochemical review of 129 cases*. Veterinary Pathology Online, 2000. **37**(6): p. 597-608.
39. Bateman, K.E., et al., *0-7-21 radiation therapy for the treatment of canine oral melanoma*. Journal of Veterinary Internal Medicine, 1994. **8**(4): p. 267-72.
40. Freeman, K.P., et al., *Treatment of dogs with oral melanoma by hypofractionated radiation therapy and platinum-based chemotherapy (1987-1997)*. Journal of Veterinary Internal Medicine, 2003. **17**(1): p. 96-101.
41. Brockley, L.K., M.A. Cooper, and P.F. Bennett, *Malignant melanoma in 63 dogs (2001-2011): the effect of carboplatin chemotherapy on survival*. New Zealand Veterinary Journal, 2013. **61**(1): p. 25-31.
42. Spugnini, E.P., et al., *Pulse-mediated chemotherapy enhances local control and survival in a spontaneous canine model of primary mucosal melanoma*. Melanoma Research, 2006. **16**(1): p. 23-7.
43. Blackwood, L. and J.M. Dobson, *Radiotherapy of oral malignant melanomas in dogs*. Journal of the American Veterinary Medical Association, 1996. **209**(1): p. 98-102.

44. Mayayo, S.L., et al., *Chondroitin sulfate proteoglycan-4: a biomarker and a potential immunotherapeutic target for canine malignant melanoma*. The Veterinary Journal, 2011. **190**(2): p. e26-30.
45. Maekawa, N., et al., *Immunohistochemical Analysis of PD-L1 Expression in Canine Malignant Cancers and PD-1 Expression on Lymphocytes in Canine Oral Melanoma*. PLoS One, 2016. **11**(6): p. e0157176.
46. Bergman, P.J., et al., *Development of a xenogeneic DNA vaccine program for canine malignant melanoma at the Animal Medical Center*. Vaccine, 2006. **24**(21): p. 4582-5.
47. Liao, J.C., et al., *Vaccination with human tyrosinase DNA induces antibody responses in dogs with advanced melanoma*. Cancer Immunology Research, 2006. **6**: p. 8.
48. Ottnod, J.M., et al., *A retrospective analysis of the efficacy of Oncept vaccine for the adjunct treatment of canine oral malignant melanoma*. Veterinary of Comparative Oncology, 2013. **11**(3): p. 219-29.
49. Yakes, F.M., et al., *Cabozantinib (XL184), a novel MET and VEGFR2 inhibitor, simultaneously suppresses metastasis, angiogenesis, and tumor growth*. Molecular Cancer Therapeutics, 2011. **10**(12): p. 2298-308.
50. U.S. Food & Drug administration. *Cabozantinib* 2012; Available from: http://www.accessdata.fda.gov/drugsatfda_docs/label/2012/203756lbl.pdf.
51. ChemieTEK. *XL 184 (FREE BASE)* Available from: <http://www.chemietek.com/xl184--free-base-details.aspx>.
52. DrugBank. *Cabozantinib*. 2017 [cited 2017; Available from: <https://www.drugbank.ca/drugs/DB08875>.
53. ClinicalTrials.gov. *cabozantinib*. 2017; Available from: <https://clinicaltrials.gov/ct2/results?term=cabozantinib&pg=1>.
54. Exelixis. *Cabozantinib*. 2017; Available from: <http://www.exelixis.com/pipeline/cabozantinib>.
55. Hubbard, S.R. and J.H. Till, *Protein tyrosine kinase structure and function*. Annual review of biochemistry, 2000. **69**(1): p. 373-398.
56. Schlessinger, J., *Cell Signaling by Receptor Tyrosine Kinases*. Cell, 2000. **103**(2): p. 211-225.
57. Takeuchi, K. and F. Ito, *Receptor tyrosine kinases and targeted cancer therapeutics*. Biological and Pharmaceutical Bulletin, 2011. **34**(12): p. 1774-1780.
58. Trusolino, L., A. Bertotti, and P.M. Comoglio, *MET signalling: principles and functions in development, organ regeneration and cancer*. Nature reviews Molecular cell biology, 2010. **11**(12): p. 834-848.
59. Danilkovitch-Miagkova, A. and B. Zbar, *Dysregulation of Met receptor tyrosine kinase activity in invasive tumors*. The Journal of clinical investigation, 2002. **109**(7): p. 863-867.

60. Rodrigues, G.A. and M. Park, *Dimerization mediated through a leucine zipper activates the oncogenic potential of the met receptor tyrosine kinase*. Molecular and Cellular Biology, 1993. **13**(11): p. 6711-22.
61. Rusciano, D., P. Lorenzoni, and M.M. Burger, *Constitutive activation of c-Met in liver metastatic B16 melanoma cells depends on both substrate adhesion and cell density and is regulated by a cytosolic tyrosine phosphatase activity*. Journal of Biological Chemistry, 1996. **271**(34): p. 20763-20769.
62. Hanahan, D. and R.A. Weinberg, *The Hallmarks of Cancer*. Cell, 2000. **100**(1): p. 57-70.
63. Carmeliet, P., *VEGF as a Key Mediator of Angiogenesis in Cancer*. Oncology, 2005. **69**(suppl 3)(Suppl. 3): p. 4-10.
64. Bergers, G. and L.E. Benjamin, *Tumorigenesis and the angiogenic switch*. Nature Reviews Cancer, 2003. **3**(6): p. 401-10.
65. Ferrara, N., *Vascular endothelial growth factor as a target for anticancer therapy*. Oncologist, 2004. **9** Suppl 1: p. 2-10.
66. Paez-Ribes, M., et al., *Antiangiogenic therapy elicits malignant progression of tumors to increased local invasion and distant metastasis*. Cancer Cell, 2009. **15**(3): p. 220-31.
67. Yu, J.L., et al., *Effect of p53 status on tumor response to antiangiogenic therapy*. Science, 2002. **295**(5559): p. 1526-8.
68. Zhang, Y., et al., *XL-184, a MET, VEGFR-2 and RET kinase inhibitor for the treatment of thyroid cancer, glioblastoma multiforme and NSCLC*. Idrugs, 2010. **13**(2): p. 112-121.
69. Kurzrock, R., et al., *Activity of XL184 (Cabozantinib), an oral tyrosine kinase inhibitor, in patients with medullary thyroid cancer*. Journal of Clinical Oncology, 2011. **29**(19): p. 2660-6.
70. DiPaola, R.S., et al., *Evidence for a functional kit receptor in melanoma, breast, and lung carcinoma cells*. Cancer gene therapy, 1996. **4**(3): p. 176-182.
71. Ronnstrand, L., *Signal transduction via the stem cell factor receptor/c-Kit*. Cellular and molecular life sciences, 2004. **61**(19-20): p. 2535-48.
72. Liang, J., et al., *The C-kit receptor-mediated signal transduction and tumor-related diseases*. International Journal of Biological Sciences, 2013. **9**(5): p. 435-443.
73. Krystal, G.W., S.J. Hines, and C.P. Organ, *Autocrine growth of small cell lung cancer mediated by coexpression of c-kit and stem cell factor*. Cancer Research, 1996. **56**(2): p. 370-6.
74. Bastian, B.C., *The molecular pathology of melanoma: an integrated taxonomy of melanocytic neoplasia*. Annual Review of Pathology: Mechanisms of Disease, 2014. **9**: p. 239-271.

75. Cohen, N.A., et al., *Pharmacological Inhibition of KIT Activates MET Signaling in Gastrointestinal Stromal Tumors*. Cancer Research, 2015. **75**(10): p. 2061.
76. Vega-Avila, E. and M.K. Pugsley. *An overview of colorimetric assay methods used to assess survival or proliferation of mammalian cells*. in *Proceedings of the Western Pharmacology Society*. 2011.
77. De Fries, R. and M. Mitsunashi, *Quantification of mitogen induced human lymphocyte proliferation: Comparison of alamarblue assay to 3h-thymidine incorporation assay*. Journal of clinical laboratory analysis, 1995. **9**(2): p. 89-95.
78. O'Brien, J., et al., *Investigation of the Alamar Blue (resazurin) fluorescent dye for the assessment of mammalian cell cytotoxicity*. European Journal of Biochemistry, 2000. **267**(17): p. 5421-5426.
79. Schmitt, D., et al., *The use of resazurin as a novel antimicrobial agent against Francisella tularensis*. Frontiers in Cellular and Infection Microbiology, 2013. **3**(93).
80. Mandy, F.F., M. Bergeron, and T. Minkus, *Principles of flow cytometry*. Transfusion Science, 1995. **16**(4): p. 303-314.
81. Roger S. Riley, M.D., Ph.D. and Michael Idowu, M.D. . *Overview of the flow cytometer* N/A; Available from: <http://www.abcam.com/protocols/introduction-to-flow-cytometry>
82. Center, R.J.C.B. *Flow Cytometry* Available from: <http://biotech.illinois.edu/flowcytometry>.
83. Michael G Ormerod. *Flow Cytometry - A Basic Introduction*. 2008; Available from: <http://flowbook.denovosoftware.com/>.
84. Vermes, I., et al., *A novel assay for apoptosis Flow cytometric detection of phosphatidylserine expression on early apoptotic cells using fluorescein labelled Annexin V*. Journal of Immunological Methods, 1995. **184**(1): p. 39-51.
85. Biosciences, B. *Detection of Apoptosis Using the BD Annexin V FITC Assay on the BD FACSVersTM System*. 2011 [cited 2017 20.05.2017]; Available from: https://www.bdbiosciences.com/documents/BD_FACSVers_Apoptosis_Detection_AppNote.pdf.
86. Blake, M.S., et al., *A rapid, sensitive method for detection of alkaline phosphatase-conjugated anti-antibody on Western blots*. Analytical Biochemistry, 1984. **136**(1): p. 175-179.
87. Kurien, B.T. and R.H. Scofield, *Western blotting*. Methods, 2006. **38**(4): p. 283-293.

88. Chon, E., et al., *Activation of the Canonical Wnt/ β -Catenin Signalling Pathway is Rare in Canine Malignant Melanoma Tissue and Cell Lines*. Journal of comparative pathology, 2013. **148**(2): p. 178-187.
89. Wei, B.R., et al., *Synergistic targeted inhibition of MEK and dual PI3K/mTOR diminishes viability and inhibits tumor growth of canine melanoma underscoring its utility as a preclinical model for human mucosal melanoma*. Pigment Cell Melanoma Res, 2016.
90. ThermoFisher. *Countess™ Automated Cell Counter Manual*. 2009; Available from: <https://tools.thermofisher.com/content/sfs/manuals/mp10227.pdf>.
91. Lee, G.Y., et al., *Three-dimensional culture models of normal and malignant breast epithelial cells*. Nature Methods, 2007. **4**(4): p. 359-65.
92. Pampaloni, F., E.G. Reynaud, and E.H. Stelzer, *The third dimension bridges the gap between cell culture and live tissue*. Nature Reviews Molecular Cell Biology, 2007. **8**(10): p. 839-45.
93. Kim, J.B., *Three-dimensional tissue culture models in cancer biology*. Seminars in Cancer Biology, 2005. **15**(5): p. 365-377.
94. Kimlin, L.C., G. Casagrande, and V.M. Virador, *In vitro three-dimensional (3D) models in cancer research: an update*. Molecular Carcinogenesis, 2013. **52**(3): p. 167-82.
95. Zhang, L., et al., *Sensitivity of neuroblastoma to the novel kinase inhibitor cabozantinib is mediated by ERK inhibition*. Cancer chemotherapy and pharmacology, 2015. **76**(5): p. 977-987.
96. Hage, C., et al., *The novel c-Met inhibitor cabozantinib overcomes gemcitabine resistance and stem cell signaling in pancreatic cancer*. Cell death & disease, 2013. **4**(5): p. e627.
97. Riss, T.L., et al., *Cell viability assays*. 2015.
98. Imamura, Y., et al., *Comparison of 2D- and 3D-culture models as drug-testing platforms in breast cancer*. Oncology Reports, 2015. **33**(4): p. 1837-43.
99. Riedl, A., et al., *Comparison of cancer cells in 2D vs 3D culture reveals differences in AKT–mTOR–S6K signaling and drug responses*. Journal of Cell Science, 2016.
100. Ohmori, T., et al., *Blockade of tumor cell transforming growth factor-betas enhances cell cycle progression and sensitizes human breast carcinoma cells to cytotoxic chemotherapy*. Experimental cell research, 1998. **245**(2): p. 350-9.
101. Li, D.-L., et al., *Anti-tumor activity of cabozantinib by FAK down-regulation in human oral squamous cell carcinoma*. Bangladesh Journal of Pharmacology, 2015. **11**(1): p. 119-125.
102. Dai, J., et al., *Cabozantinib inhibits prostate cancer growth and prevents tumor-induced bone lesions*. Clinical Cancer Research, 2014. **20**(3): p. 617-30.
103. Song, E.-K., et al., *Potent antitumor activity of Cabozantinib, a c-MET and VEGFR2 Inhibitor, in a Colorectal Cancer Patient-derived Tumor Explant*

- Model*. International journal of cancer. Journal international du cancer, 2015. **136**(8): p. 1967-1975.
104. Lin, H., et al., *2ME2 inhibits the activated hypoxia-inducible pathways by cabozantinib and enhances its efficacy against medullary thyroid carcinoma*. Tumor Biology, 2016. **37**(1): p. 381-391.
 105. Ruan, M., et al., *Iodide-and glucose-handling gene expression regulated by sorafenib or cabozantinib in papillary thyroid cancer*. The Journal of Clinical Endocrinology & Metabolism, 2015. **100**(5): p. 1771-1779.
 106. Xiang, Q., et al., *Cabozantinib suppresses tumor growth and metastasis in hepatocellular carcinoma by a dual blockade of VEGFR2 and MET*. Clinical Cancer Research, 2014. **20**(11): p. 2959-70.
 107. Giles, R.H., J.H. van Es, and H. Clevers, *Caught up in a Wnt storm: Wnt signaling in cancer*. Biochim Biophys Acta, 2003. **1653**(1): p. 1-24.
 108. Ysebaert, L., et al., *Expression of beta-catenin by acute myeloid leukemia cells predicts enhanced clonogenic capacities and poor prognosis*. Leukemia, 2006. **20**(7): p. 1211-6.
 109. Kent, M.S., C.J. Collins, and F. Ye, *Activation of the AKT and mammalian target of rapamycin pathways and the inhibitory effects of rapamycin on those pathways in canine malignant melanoma cell lines*. American journal of veterinary research, 2009. **70**(2): p. 263-269.
 110. Abbott, A., *Cancer: the root of the problem*. Nature, 2006. **442**(7104): p. 742-3.
 111. Liu, L., et al., *Enrichment of c-Met+ tumorigenic stromal cells of giant cell tumor of bone and targeting by cabozantinib*. Cell death & disease, 2014. **5**(10): p. e1471.
 112. Navis, A.C., et al., *Effects of dual targeting of tumor cells and stroma in human glioblastoma xenografts with a tyrosine kinase inhibitor against c-MET and VEGFR2*. PloS one, 2013. **8**(3): p. e58262.
 113. Bottaro, D.P. and L.A. Liotta, *Cancer: Out of air is not out of action*. Nature, 2003. **423**(6940): p. 593-5.
 114. Ebos, J.M., et al., *Accelerated metastasis after short-term treatment with a potent inhibitor of tumor angiogenesis*. Cancer Cell, 2009. **15**(3): p. 232-9.
 115. Iqbal, N. and N. Iqbal, *Imatinib: a breakthrough of targeted therapy in cancer*. Chemotherapy research and practice, 2014. **2014**.
 116. Exelixis. *Clinical Development Collaborations Pairing Cabozantinib with Immunotherapies*. 2017; Available from: <http://www.exelixis.com/pipeline/cabozantinib>.